

Motion of charged test particles in Reissner-Nordström spacetime

 Daniela Pugliese,^{1,2,*} Hernando Quevedo,^{1,3,†} and Remo Ruffini^{1,‡}
¹*Dipartimento di Fisica, Università di Roma La Sapienza, Piazzale Aldo Moro 5, I-00185 Roma, Italy
and ICRA Net, Piazzale della Repubblica 10, I-65122 Pescara, Italy*
²*School of Mathematical Sciences, Queen Mary, University of London, Mile End Road, London E1 4NS, United Kingdom*
³*Instituto de Ciencias Nucleares, Universidad Nacional Autónoma de México, AP 70543, México, DF 04510, Mexico*
(Received 24 January 2011; revised manuscript received 6 April 2011; published 27 May 2011)

We investigate the circular motion of charged test particles in the gravitational field of a charged mass described by the Reissner-Nordström spacetime. We study in detail all the spatial regions where circular motion is allowed around either black holes or naked singularities. The effects of repulsive gravity are discussed by finding all the circles at which a particle can have vanishing angular momentum. We show that the geometric structure of stable accretion disks, made of only test particles moving along circular orbits around the central body, allows us to clearly distinguish between black holes and naked singularities.

DOI: 10.1103/PhysRevD.83.104052

PACS numbers: 04.20.-q, 04.40.Dg, 04.70.Bw

I. INTRODUCTION

Let us consider the background of a static gravitational source of mass M and charge Q , described by the Reissner-Nordström (RN) line element in standard spherical coordinates

$$ds^2 = -\frac{\Delta}{r^2} dt^2 + \frac{r^2}{\Delta} dr^2 + r^2(d\theta^2 + \sin^2\theta d\phi^2), \quad (1)$$

where $\Delta = (r - r_+)(r - r_-)$ and $r_{\pm} = M \pm \sqrt{M^2 - Q^2}$ are the radii of the outer and inner horizon, respectively. Furthermore, the associated electromagnetic potential and field are

$$A = \frac{Q}{r} dt, \quad F = dA = -\frac{Q}{r^2} dt \wedge dr, \quad (2)$$

respectively.

The motion of a test particle of charge q and mass μ moving in a RN background (1) is described by the following Lagrangian density:

$$\mathcal{L} = \frac{1}{2} g_{\alpha\beta} \dot{x}^\alpha \dot{x}^\beta + \epsilon A_\alpha \dot{x}^\alpha, \quad (3)$$

where A_α are the components of the electromagnetic 4-potential, the dot represents differentiation with respect to the proper time, and the parameter $\epsilon = q/\mu$ is the specific charge of the test particle. The equations of motion of the test particle can be derived from Eq. (3) by using the Euler-Lagrange equation. Then,

$$\dot{x}^\alpha \nabla_\alpha \dot{x}^\beta = \epsilon F^\beta{}_\gamma \dot{x}^\gamma, \quad (4)$$

where $F_{\alpha\beta} \equiv A_{\alpha,\beta} - A_{\beta,\alpha}$.

Since the Lagrangian density (3) does not depend explicitly on the variables t and ϕ , the following two conserved quantities exist

$$p_t \equiv \frac{\partial \mathcal{L}}{\partial \dot{t}} = -\left(\frac{\Delta}{r^2} \dot{t} + \frac{\epsilon Q}{r}\right) = -\frac{E}{\mu}, \quad (5)$$

$$p_\phi = \frac{\partial \mathcal{L}}{\partial \dot{\phi}} = r^2 \sin^2\theta \dot{\phi} = \frac{L}{\mu}, \quad (6)$$

where L and E are, respectively, the angular momentum and energy of the particle as measured by an observer at rest at infinity. Moreover, to study the motion of charged test particles in the RN spacetime it is convenient to use the fact if the initial position and the tangent vector of the trajectory of the particle lie on a plane that contains the center of the body, then the entire trajectory must lie on this plane. Without loss of generality we may therefore restrict ourselves to the study of equatorial trajectories with $\theta = \pi/2$.

On the equatorial plane $\theta = \pi/2$, the motion equations can be reduced to the form $\dot{r}^2 + V^2 = E^2/\mu^2$, which describes the motion inside an effective potential V . Then, we define the potential

$$V_{\pm} = \frac{E^{\pm}}{\mu} = \frac{\epsilon Q}{r} \pm \sqrt{\left(1 + \frac{L^2}{\mu^2 r^2}\right) \left(1 - \frac{2M}{r} + \frac{Q^2}{r^2}\right)} \quad (7)$$

as the value of E/μ that makes r into a ‘‘turning point’’ ($V = E/\mu$); in other words, the value of E/μ at which the (radial) kinetic energy of the particle vanishes [1–4]. The effective potential with positive (negative) sign corresponds to the solution with

$$\lim_{r \rightarrow \infty} E^+ = +\mu; \quad \lim_{r \rightarrow \infty} E^- = -\mu,$$

where

$$E^+(L, \epsilon, r) \geq E^-(L, \epsilon, r), \quad (8)$$

*d.pugliese.physics@gmail.com,

†quevedo@nucleares.unam.mx,

‡ruffini@icra.it

and the following relation holds:

$$E^+(L, \epsilon, r) = -E^-(L, -\epsilon, r). \quad (9)$$

The behavior of the effective potential strongly depends on the sign of ϵQ ; in particular, in the case of $\epsilon Q < 0$, negative energy states for the solution E^+ can exist (see also [5–11]).

The problem of finding exact solutions of the motion equations of test particles moving in a RN spacetime has been widely studied in literature in many contexts and ways. For a recent discussion, we mention the works [5–11]. In particular, in a recent paper [5], the full set of analytical solutions of the motion equations for electrically and magnetically charged test particles is discussed in terms of the Weierstrass (γ , σ and ζ) functions. The general structure of the geodesics was discussed and a classification of their types was proposed. Remarkably, analytical solutions are found in the case of a central RN source not only with constant electric charge, but also with constant magnetic charge. It is interesting to notice that if either the test particle or the central body possesses both types of charge, it turns out that the motion is no longer confined to a plane. In the present work, we consider only equatorial circular orbits around a central RN source with constant electric charge. Instead of solving directly the equations of motion, we explore the properties of the effective potential function associated to the motion. Thus, we discuss and propose a classification of the equatorial orbits in terms of the two constants of motion: the energy E/μ and the orbital angular momentum $L/(\mu M)$. In fact, we focus our attention on some peculiar features of the circular motion and the physics around black holes and naked singularities. In particular, we are interested in exploring the possibility of distinguishing between black holes and naked singularities by studying the motion of circular test particles. In this sense, the present work complements and is different from previous studies [5–11].

In a previous work [12,13], we analyzed the dynamics of the RN spacetime by studying the motion of neutral test particles for which the effective potential turns out to coincide with V_+ as given in Eq. (7) with $\epsilon = 0$. We will see that in the case of charged test particles the term $\epsilon Q/r$ drastically changes the behavior of the effective potential, and leads to several possibilities which must be analyzed in the case of black holes and naked singularities. In particular, we will show that for particles moving along circular orbits there exist stability regions whose geometric structure clearly distinguishes naked singularities from black holes (see also [14–17]). The plan of this paper is the following: In Sec. II, we investigate the behavior of the effective potential and the conditions for the motion of positive and negative charged test particles moving on circular orbits around the central charged mass. This section also contains a brief analysis of the Coulomb approximation of the effective potential. In Sec. III, we will

consider the black hole case while in Sec. IV, we shall focus on the motion around naked singularities. The conclusions are in Sec. V.

II. CIRCULAR MOTION

The circular motion of charged test particles is governed by the behavior of the effective potential (7). In this work, we will mainly consider the special case of a positive solution V_+ for the potential in order to be able to compare our results with those obtained in the case of neutral test particles analyzed in [12,13]. Thus, the radius of circular orbits and the corresponding values of the energy E and the angular momentum L are given by the extrema of the function V_+ . Therefore, the conditions for the occurrence of circular orbits are:

$$\frac{dV_+}{dr} = 0, \quad V_+ = \frac{E^+}{\mu}. \quad (10)$$

When possible, to simplify the notation we will drop the subindex (+) so that, for example, $V = E/\mu$ will denote the positive effective potential solution. Solving Eq. (10) with respect to L , we find the specific angular momentum

$$\frac{(L^\pm)^2}{\mu^2} = \frac{r^2}{2\Sigma^2} \left[2(Mr - Q^2)\Sigma + \epsilon^2 Q^2 \Delta \pm Q\Delta \sqrt{\epsilon^2(4\Sigma + \epsilon^2 Q^2)} \right], \quad (11)$$

where $\Sigma \equiv r^2 - 3Mr + 2Q^2$, of the test particle on a circular orbit of radius r . The corresponding energy can be obtained by introducing the expression for the angular momentum into Eq. (7). Then, we obtain

$$\frac{E^\pm}{\mu} = \frac{\epsilon Q}{r} + \frac{\Delta \sqrt{2\Sigma + \epsilon^2 Q^2 \pm Q\sqrt{\epsilon^2(4\Sigma + \epsilon^2 Q^2)}}}{\sqrt{2}r|\Sigma|}. \quad (12)$$

The sign in front of the square root should be chosen in accordance with the physical situation. This point will be clarified below by using the formalism of orthonormal frames.

An interesting particular orbit is the one in which the particle is located at rest as seen by an observer at infinity, i.e., $L = 0$. These ‘‘orbits’’ are therefore characterized by the following conditions:

$$L = 0, \quad \frac{dV}{dr} = 0. \quad (13)$$

[18]. Solving Eq. (13) for $Q \neq 0$ and $\epsilon \neq 0$, we find the following radius

$$r_s^\pm \equiv \frac{(\epsilon^2 - 1)Q^2 M}{\epsilon^2 Q^2 - M^2} \pm \sqrt{\frac{\epsilon^2 Q^4 (\epsilon^2 - 1)(M^2 - Q^2)}{(\epsilon^2 Q^2 - M^2)^2}}. \quad (14)$$

TABLE I. Radii of the orbits characterized by the conditions $L = 0$ and $dV/dr = 0$.

$0 < Q < M$		$Q = M$		$Q > M$	
ϵ	Radius	ϵ	Radius	ϵ	Radius
$\epsilon > M/Q$	$r = r_s^+$	$\epsilon = 1$	$r > M$	$-M/Q < \epsilon < 0$	$r = r_s^-$
				$\epsilon = -M/Q$	$r = Q^2/(2M)$
				$-1 < \epsilon \leq -M/Q$	$r = r_s^+$
				$\epsilon = 0$	$r = Q^2/M$
				$0 < \epsilon < M/Q$	$r = r_s^+$

Table I shows the explicit values of all possible radii for different values of the ratio Q/M . A particle located at $r = r_s$ with angular momentum $L = 0$ will have the energy (see also [18–24])

$$\frac{E_s^\pm}{\mu} \equiv \frac{1}{Q} \left(\sqrt{\frac{M^2 - Q^2}{\epsilon^2 - 1}} + \frac{\epsilon}{\frac{\epsilon^2 - 1}{\epsilon^2 Q^2 - M^2} \pm \sqrt{\frac{\epsilon^2(M^2 - Q^2)(\epsilon^2 - 1)}{(\epsilon^2 Q^2 - M^2)^2}}} \right). \quad (15)$$

The minimum radius for a stable circular orbit occurs at the inflection points of the effective potential function; thus, we must solve the equation

$$\frac{d^2V}{dr^2} = 0, \quad (16)$$

for the orbit radius r , using the expression (11) for the angular momentum L . From Eq. (10) and (16) we find that the radius of the last stable circular orbit and the angular momentum of this orbit are related by the following equations

$$\begin{aligned} & (L^2 + Q^2 - 1)r^6 - 6L^2r^5 + 6L^2(1 + Q^2)r^4 \\ & - 2L^2(2L^2 + 5Q^2)r^3 + L^2(3L^2 + 3L^2Q^2 + 3Q^4) \\ & \times r^2 - 6L^4Q^2r + 2L^4Q^4 = 0, \end{aligned}$$

and

$$\begin{aligned} & Q^2r^2 - r^3 + L^2(2Q^2 - 3r + r^2) \\ & + Qr^3 \sqrt{\frac{(L^2 + r^2)(Q^2 - 2r + r^2)}{r^4}} \epsilon = 0, \quad (17) \end{aligned}$$

where in order to simplify the notation we introduced the normalized quantities $L \rightarrow L/(M/\mu)$, $r \rightarrow r/M$, and $Q \rightarrow Q/M$. Equation (17) depends on the test particle specific charge ϵ via the function L as given in Eq. (11). It is possible to solve Eq. (17) for the last stable circular orbit radius as a function of the free parameter L . We find the expression

$$\begin{aligned} \frac{(L_{\text{lsc}}^\pm)^2}{\mu^2} &= \frac{r^2}{2[2Q^4 + 3Q^2r(r-2M) - (2r-3M)r^2]} \\ &\times [2Q^2(5M-3r)r - 3Q^4 - r^2[6M^2 + (r-6M)r] \\ &\pm \sqrt{9Q^2 + (r-6M)r(Q^2 + (r-2M)r)^{3/2}}] \quad (18) \end{aligned}$$

for the angular momentum of last stable circular orbit. Equation (18) can be substituted in Eq. (17) to find the radius of the last stable circular orbit.

Coulomb potential approximation

Consider the case of a charged particle moving in the Coulomb potential

$$U(r) = \frac{Q}{r}.$$

This means that we are considering the motion described by the following effective potential

$$V_+ = \frac{E^+}{\mu} = \frac{\epsilon Q}{r} + \sqrt{1 + \frac{L^2}{\mu^2 r^2}}, \quad (19)$$

where $\epsilon Q < 0$. The Coulomb approximation is interesting for our further analysis because it corresponds to the limiting case for large values of the radial coordinate r [cf. Equation (7)].

Circular orbits are therefore situated at $r = r_c$ with

$$r_c = \sqrt{\frac{L^2}{\mu^2} \left(\frac{L^2}{\epsilon^2 Q^2} - 1 \right)} \quad \text{and} \quad \frac{L^2}{\mu^2} \geq \epsilon^2 Q^2, \quad (20)$$

and in the case $\epsilon = 0$ with $Q > 0$, circular orbits exist in all $r > 0$ for $L = 0$. We conclude that in this approximation circular orbits always exist with orbital radius r_c and angular momentum satisfying the condition $|L|/\mu \geq |\epsilon Q|$. For the last stable circular orbit situated at $r = r_{\text{lsc}}$ we find

$$r_{\text{lsc}} = 0 \quad \text{with} \quad \frac{E^+(r_{\text{lsc}})}{\mu} = 0 \quad \text{and} \quad \frac{|L|}{\mu} = |\epsilon Q|. \quad (21)$$

This means that, in the approximation of the Coulomb potential, all the circular orbits are stable, including the limiting case of a particle at rest on the origin of coordinates.

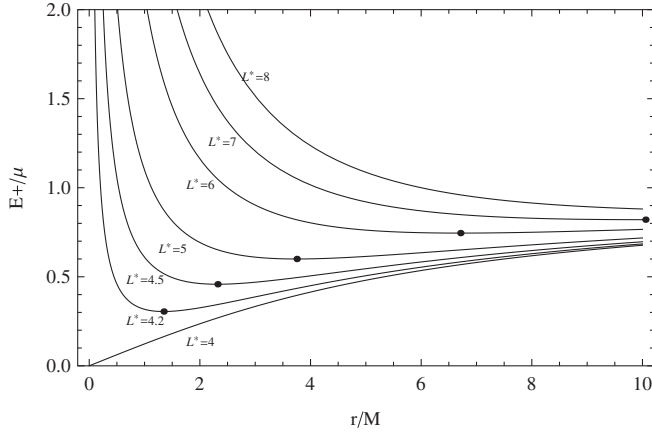


FIG. 1. Effective potential for a charged test particle with $\epsilon = -2$ moving in a Coulomb potential with $Q/M = 2$ for different values of the momentum $L^* \equiv L/(\mu M)$. The points indicate the minima of the potential. In particular, for $L^* = |\epsilon Q|/M$ the potential vanishes on the origin $r = 0$ (see text).

Furthermore, Eqs. (20) and (21) show that, in contrast with the general RN case, for a charged particle moving in a Coulomb potential only positive or null energy solutions can exist. See Fig. 1 where the potential (19) is plotted as a function of the orbital radius for different values of the angular momentum.

III. BLACK HOLES

In the case of a black hole ($M^2 > Q^2$), the two roots V_{\pm} of the effective potential are plotted as a function of the ratio r/M in Fig. 2 for a fixed value of the charge-to-mass

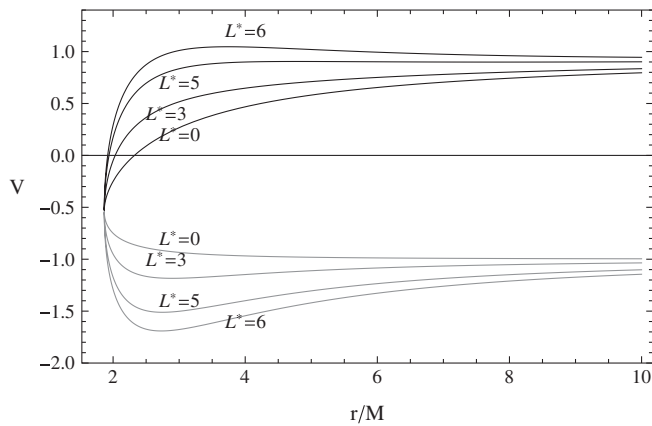


FIG. 2. The effective potential as a function of r/M for a charged particle of charge-to-mass ratio $\epsilon \equiv q/\mu$ moving in a Reissner-Nordström black hole of charge Q and mass M . The graphic shows the positive E^+/μ (black curves) and negative roots E^-/μ (gray curves) of the effective potential for $Q/M = 0.5$, $\epsilon = -2$, and different values of the momentum $L^* \equiv L/(M\mu)$. The outer horizon is located at $r_+ \equiv M + \sqrt{M^2 - Q^2} \approx 1.87M$. Note the presence of negative energy states for the positive roots.

ratio of the test particle and different values of the angular momentum $L/(M\mu)$ (see also [25–30]). Notice the presence of negative energy states for the positive solution $V_+ = E^+/\mu$ of the effective potential function. Negative energy states for V_+ are possible only in the case $\epsilon Q < 0$. In particular, the largest region in which the V_+ solution has negative energy states is

$$M + \sqrt{M^2 - Q^2} < r \leq M + \sqrt{M^2 - Q^2(1 - \epsilon^2)} \quad (22)$$

and corresponds to the limiting case of vanishing angular momentum ($L = 0$). For $L \neq 0$, this region becomes smaller and decreases as L increases. For a given value of the orbit radius, say r_0 , such that $r_0 < M + \sqrt{M^2 - Q^2(1 - \epsilon^2)}$, the angular momentum of the test particle must be chosen within the interval

$$0 < \frac{L^2}{\mu^2} < r_0^2 \left(\frac{\epsilon^2 Q^2}{r_0^2 - 2Mr_0 + Q^2} - 1 \right) \quad (23)$$

for a region with negative energy states to exist. This behavior is illustrated in Fig. 2.

Figure 3 shows the positive solution V_+ of the effective potential for different values of the momentum and for positive and negative charged particles. In particular, we note that, at fixed Q/M for a particle with $|\epsilon| < 1$, in the case $\epsilon Q > 0$ the stable orbit radius is larger than in the case of attractive electromagnetic interaction, i. e., $\epsilon Q < 0$. In Fig. 4, the potential V_+ of an extreme black hole is plotted for different positive and negative values of the test particle with charge-to-mass ratio ϵ . In this case, it is clear that the magnitude of the energy increases as the magnitude of the specific charge of the particle ϵ increases.

As mentioned in Sec. II, in the case of the positive solution for the effective potential, the conditions for the existence of circular orbits

$$\dot{r} = 0, \quad V = \frac{E}{\mu}, \quad \frac{dV}{dr} = 0 \quad (24)$$

lead to Eqs. (11) and (12), in which the selection of the (\pm) sign inside the square root should be done properly. To clarify this point, we consider explicitly the equation of motion for a charged particle in the gravitational field of a RN black hole.

$$a(U)^\alpha = \epsilon F^\alpha{}_\beta U^\beta, \quad (25)$$

where $a(U) = \nabla_U U$ is the particle's 4-acceleration. Introducing the orthonormal frame

$$\begin{aligned} e_{\hat{t}} &= \frac{r}{\Delta^{1/2}} \partial_t, & e_{\hat{r}} &= \frac{\Delta^{1/2}}{r} \partial_r, \\ e_{\hat{\theta}} &= \frac{1}{r} \partial_\theta, & e_{\hat{\phi}} &= \frac{1}{r \sin\theta} \partial_\phi, \end{aligned} \quad (26)$$

with dual

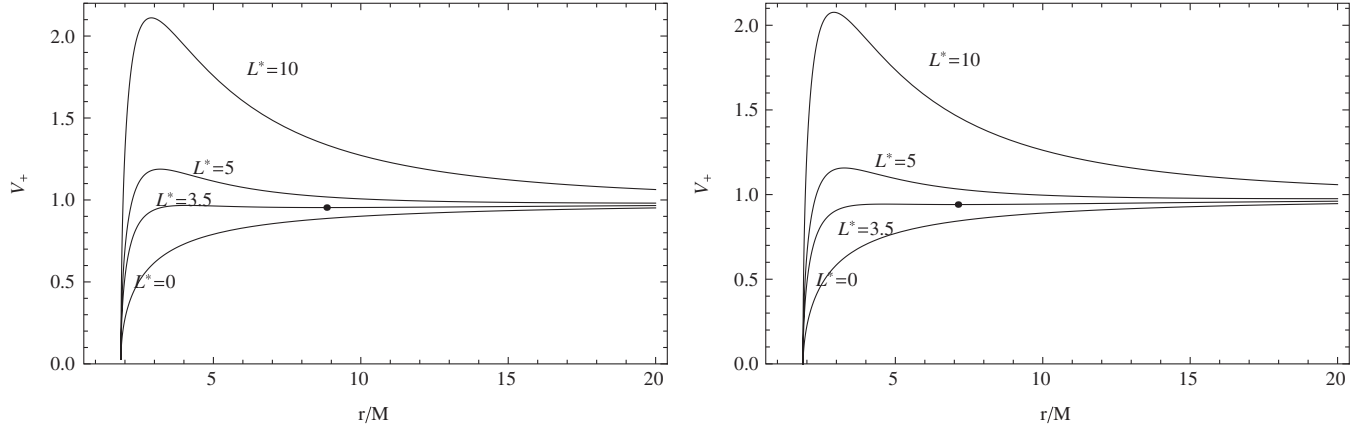


FIG. 3. The effective potential V_+ for a charged particle of charge-to-mass ratio, $\epsilon = q/\mu$, moving in a Reissner-Nordström spacetime of charge Q and mass M with charge-to-mass ratio $Q/M = 0.5$ is plotted as a function of the radial coordinate r/M for different values of the angular momentum $L^* \equiv L/(M\mu)$. The outer horizon is located at $r_+ \approx 1.87M$. In the graphic on the left with $\epsilon = 0.1$, the effective potential for $L^* \approx 3.5$ has a minimum $V_{\min} \approx 0.954$ at $r_{\min} \approx 8.84M$. In the graphic on the right with $\epsilon = -0.1$, the minimum $V_{\min} \approx 0.94$ is located at $r_{\min} \approx 7.13M$ for $L^* \approx 3.5$.

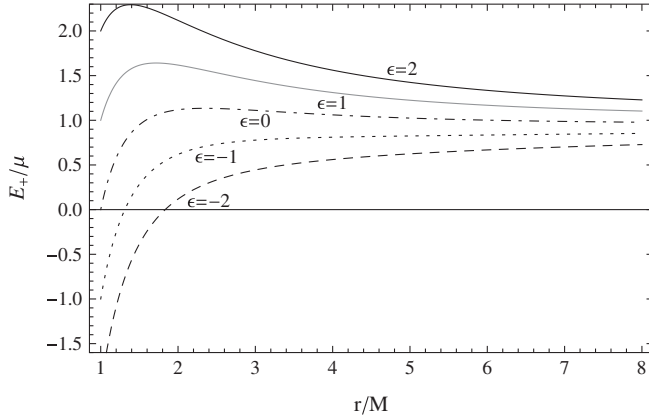


FIG. 4. The effective potential V_+ is plotted as a function of r/M for a charged test particle with specific charge $\epsilon = q/\mu$ moving in the field of a Reissner-Nordström extreme black hole ($Q = M$). Here $L/(M\mu) = 4$, and the effective potential is plotted for different values of ϵ . The outer horizon is located at $r_+ \equiv M + \sqrt{M^2 - Q^2} = M$. Note the presence of negative energy states for particles with negative ϵ .

$$\begin{aligned} \omega^{\hat{t}} &= \frac{\Delta^{1/2}}{r} dt, & \omega^{\hat{r}} &= \frac{r}{\Delta^{1/2}} dr, \\ \omega^{\hat{\theta}} &= r d\theta, & \omega^{\hat{\phi}} &= r \sin\theta d\phi; \end{aligned} \quad (27)$$

the tangent to a (timelike) spatially circular orbit u^α can be expressed as

$$u = \Gamma(\partial_t + \zeta \partial_\phi) = \gamma(e_{\hat{t}} + \nu e_{\hat{\phi}}),$$

where Γ and γ are normalization factors

$$\Gamma^2 = (-g_{tt} - \zeta^2 g_{\phi\phi})^{-1} \quad \text{and} \quad \gamma^2 = (1 - \nu^2)^{-1},$$

which guarantees that $u_\alpha u^\alpha = -1$. Here ζ is the angular velocity with respect to infinity and ν is the “local proper linear velocity” as measured by an observer associated with the orthonormal frame. The angular velocity ζ is related to the local proper linear velocity by

$$\zeta = \sqrt{\frac{-g_{tt}}{g_{\phi\phi}}} \nu.$$

Since only the radial component of the 4-velocity is non-vanishing, Eq. (25) can be written explicitly as

$$0 = \gamma(\nu^2 - \nu_g^2) + \frac{\nu_g}{\zeta_g} \frac{\epsilon Q}{r^2}, \quad (28)$$

where

$$\zeta_g = \pm \frac{\sqrt{Mr - Q^2}}{r^2}, \quad \nu_g = \sqrt{\frac{Mr - Q^2}{\Delta}}. \quad (29)$$

This equation gives the values of the particle linear velocity $\nu = \pm \nu_\epsilon^\pm$, which are compatible with a given value of ϵQ on a circular orbit of radius r , i. e.,

$$\nu_\epsilon^\pm = \nu_g \sqrt{1 - \frac{Q^2 \epsilon^2}{2r^4 \zeta_g^2} \pm \frac{Q}{r^2 \zeta_g \nu_g} \sqrt{\gamma_g^2 + \frac{Q^2 \epsilon^4 \nu_g^2}{4r^4 \zeta_g^2}}}, \quad (30)$$

where

$$\gamma_g = \left(\frac{\Delta}{r^2 - 3Mr + 2Q^2} \right)^{1/2},$$

and

$$\gamma_\epsilon^\pm = (1 - \nu_\epsilon^\pm)^{-1/2}. \quad (31)$$

In the limiting case of a neutral particle ($\epsilon = 0$), Eq. (28) implies that the linear velocity of the particle is ν_g .

We introduce the limiting value of the parameter ϵ corresponding to a particle at rest, $\nu = 0$, in Eq. (28), i. e.,

$$\epsilon_0 = \nu_g \zeta_g \frac{r^2}{Q} = \frac{Mr - Q^2}{Q\sqrt{\Lambda}}. \quad (32)$$

By introducing this quantity into Eq. (28), one gets the following equivalent relation

$$\frac{\epsilon}{\epsilon_0} = \gamma \left(1 - \frac{\nu^2}{\nu_g^2} \right), \quad (33)$$

whose solution (30) can be conveniently rewritten as

$$\nu_\epsilon^\pm = \nu_g \left[\Lambda \pm \sqrt{\Lambda^2 - 1 + (\epsilon/\epsilon_0)^2} \right]^{1/2}, \quad (34)$$

where

$$\Lambda = 1 - \frac{\nu_g^2}{2} \left(\frac{\epsilon}{\epsilon_0} \right)^2. \quad (35)$$

Moreover, from Eq. (33) it follows that $\epsilon < 0$ implies that $\nu^2 > \nu_g^2$ (because ϵ_0 is always positive for $r > r_+$), so that the allowed solutions for ν can exist only for $r \geq r_\gamma^+$, where

$$r_\gamma^+ \equiv \frac{1}{2} \left(3M + \sqrt{9M^2 - 8Q^2} \right), \quad (36)$$

the equality corresponding to $\nu_g = 1$. In this case, the solutions of Eq. (28) are given by $\nu = \pm \nu_\epsilon^+$.

For $\epsilon > 0$, instead, solutions can exist also for $r_+ < r < r_\gamma^+$. The situation strongly depends on the considered range of values of ϵ and is summarized below.

Equation (34) gives the following conditions for the existence of velocities

$$\Lambda^2 - 1 + (\epsilon/\epsilon_0)^2 \geq 0, \quad (37)$$

$$\Lambda \pm \sqrt{\Lambda^2 - 1 + (\epsilon/\epsilon_0)^2} \geq 0. \quad (38)$$

The second condition, Eq. (38), is satisfied by

$$r \geq r_l \equiv \frac{3M}{2} + \frac{1}{2} \sqrt{9M^2 - 8Q^2 - \epsilon^2 Q^2}. \quad (39)$$

Moreover, for $Q = M$ and $\epsilon = 1$, it is $\Lambda + \sqrt{\Lambda^2 - 1 + (\epsilon/\epsilon_0)^2} \geq 0$ when $M < r < (3/2)M$. However, it is also possible to show that condition Eq. (10) is satisfied for $0 < Q < M$ and $\epsilon > 0$ only in the range $r \geq r_l$.

Requiring that the argument of the square root be non-negative implies

$$\epsilon \leq \epsilon_l \equiv \frac{\sqrt{9M^2 - 8Q^2}}{Q}. \quad (40)$$

The condition (38) will be discussed later.

From the equation of motion (33) it follows that the velocity vanishes for $\epsilon/\epsilon_0 = 1$, i. e., for [cf. Eq. (14)]

$$\begin{aligned} r &= r_s \\ &\equiv \frac{Q^2}{\epsilon^2 Q^2 - M^2} \left[M(\epsilon^2 - 1) + \sqrt{\epsilon^2(\epsilon^2 - 1)(M^2 - Q^2)} \right], \end{aligned} \quad (41)$$

which exists only for $\epsilon > M/Q$. We thus have that

$$\frac{\epsilon}{\epsilon_0} > 1 \quad \text{for } r > r_s, \quad (42)$$

whereas

$$\frac{\epsilon}{\epsilon_0} < 1 \quad \text{for } r_+ < r < r_s. \quad (43)$$

On the other hand, the condition $\nu = 0$ in Eq. (34) implies that

$$\left[\Lambda \pm \sqrt{\Lambda^2 - 1 + (\epsilon/\epsilon_0)^2} \right]_{\epsilon/\epsilon_0=1} = 0, \quad (44)$$

$$\text{i. e. } \left[\Lambda \pm \sqrt{\Lambda^2 - 1} \right]_{r=r_s} = 0; \quad (45)$$

thus, ν_ϵ^- is identically zero whereas $\nu_\epsilon^+ = 2\Lambda(r_s) = 0$ only for

$$\epsilon = \tilde{\epsilon} \equiv \frac{1}{\sqrt{2}Q} \sqrt{5M^2 - 4Q^2 + \sqrt{25M^2 - 24Q^2}}. \quad (46)$$

Finally, the lightlike condition $\nu = 1$ is reached only at $r = r_\gamma^+$, where $\nu_g = 1 = \nu$.

The behavior of charged test particles depends very strongly on their location with respect to the special radii r_+ , r_l , r_γ^+ , and r_s . In Sec. III, the behavior of these radii will be analyzed in connection with the problem of stability of circular orbits.

On the other hand, the particle's 4-momentum is given by $P = mU - qA$. Then, the conserved quantities associated with the temporal and azimuthal Killing vectors $\xi = \partial_t$ and $\eta = \partial_\phi$ are, respectively,

$$P \cdot \xi = -\frac{\epsilon Q}{r} - \gamma \frac{\sqrt{\Lambda}}{r} = -\frac{E}{\mu}, \quad (47)$$

$$P \cdot \eta = \frac{r}{M} \gamma \nu = \frac{L}{M\mu}, \quad (48)$$

where E/μ and L/μ are the particle's energy and angular momentum per unit mass, respectively, (see also Eqs. (11) and (12)).

Let us summarize the results.

1. Case $\epsilon < 0$

The solutions are the geodesic velocities $\nu = \pm \nu_\epsilon^+$ in the range $r \geq r_\gamma^+$ as illustrated in Fig. 5. Orbits with radius $r = r_\gamma^+$ are lightlike. We can also compare the velocity of

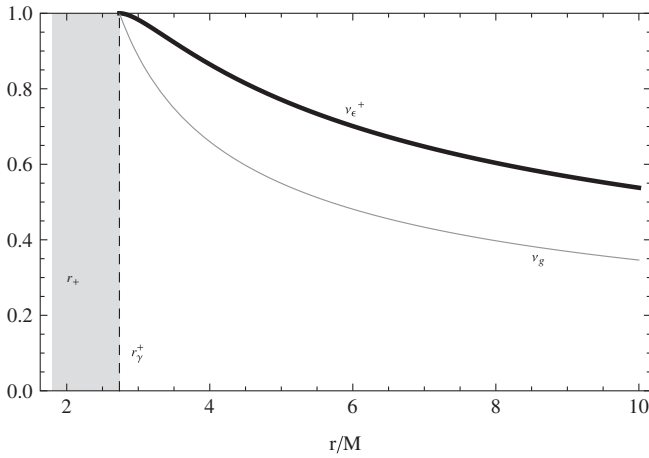


FIG. 5. The positive solution of the linear velocity v_ϵ^+ is plotted as a function of the radial distance r/M for the parameter choice $Q/M = 0.6$ and $\epsilon = -3$ so that $r_\gamma^+/M \approx 2.74$ and the outer horizon is located at $r_+/M = 1.8$. The geodesic velocity v_g is also shown (gray curve). The shaded region ($r < r_\gamma^+$) is forbidden.

charged test particles with the geodesic velocity v_g for neutral particles. For $r > r_\gamma^+$, we see that $v_\epsilon^+ > v_g$ always. This means that, at fixed orbital radius, charged test particles acquire a larger orbital velocity compared to that of neutral test particles in the same orbit. As it is possible to see from Eq. (30) and also in Fig. 6, an increase in the particle charge $\epsilon < 0$ corresponds to an increase in the

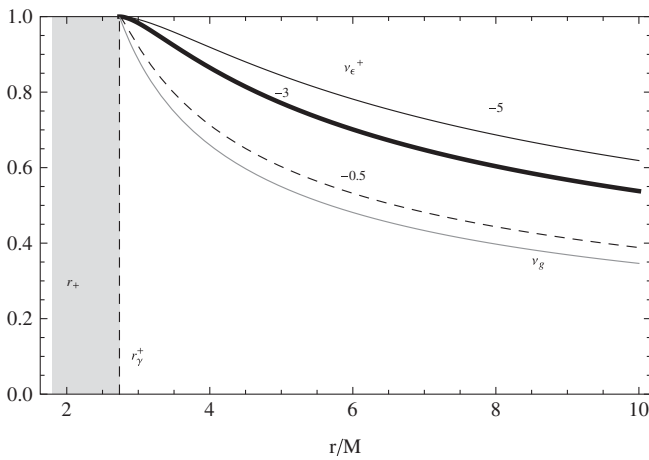


FIG. 6. The positive solution of the linear velocity v_ϵ^+ is plotted as a function of the radial distance r/M for the parameter choice $Q/M = 0.6$ and different values of $\epsilon = -5$ (black curve), $\epsilon = -3$ (thick black curve), and $\epsilon = -0.5$ (dashed curve). The geodesic velocity v_g for $\epsilon = 0$ is also shown (gray curve). The choice of parameters implies that $r_\gamma^+/M \approx 2.74$ and the outer horizon is located at $r_+/M = 1.8$. The shaded region is forbidden. For $r > r_\gamma^+$ it holds that $v_\epsilon^+ > v_g$.

velocity v_ϵ^+ . As the orbital radius decreases, the velocity increases until it reaches the limiting value $v_\epsilon^+ = 1$, which corresponds to the velocity of a photon. This fact can be seen also in Fig. 7, where the energy and angular momentum for circular orbits are plotted in terms of the distance r . Clearly, this graphic shows that to reach the photon orbit at $r = r_\gamma^+$, the particles must acquire an infinity amount of energy and angular momentum. In Fig. 8 we analyze the behavior of the particle's energy and angular momentum in terms of the specific charge ϵ . It follows that both quantities decrease as the value of $|\epsilon|$ decreases.

2. Case $\epsilon = 0$

The solutions are the geodesic velocities $v = \pm v_g$ in the range $r \geq r_\gamma^+$. This case has been studied in detail in [12].

3. Case $\epsilon > 0$

Depending on the explicit values of the parameters Q and ϵ and the radial coordinate r , it is necessary to analyze several subcases.

(a) $\epsilon < M/Q$ and $r \geq r_l$.

There are two different branches for both signs of the linear velocity: $v = \pm v_\epsilon^+$ in the range $r_l \leq r \leq r_\gamma^+$, and $v = \pm v_\epsilon^-$ in the whole range $r \geq r_l$. The two branches join at $r = r_l$, where $v_\epsilon^+ = v_\epsilon^- = v_g \sqrt{\Lambda}$, as shown in Fig. 9. First, we note that in this case for $r > r_\gamma^+$ it always holds that $v_\epsilon^- < v_g$. This means that, at fixed orbital radius, charged test particles possess a smaller orbital velocity than that of neutral test particles in the same orbit. This is in accordance to the fact that in this case, a black hole with $\epsilon Q > 0$, the attractive gravitational force is balanced by the repulsive electromagnetic force. In

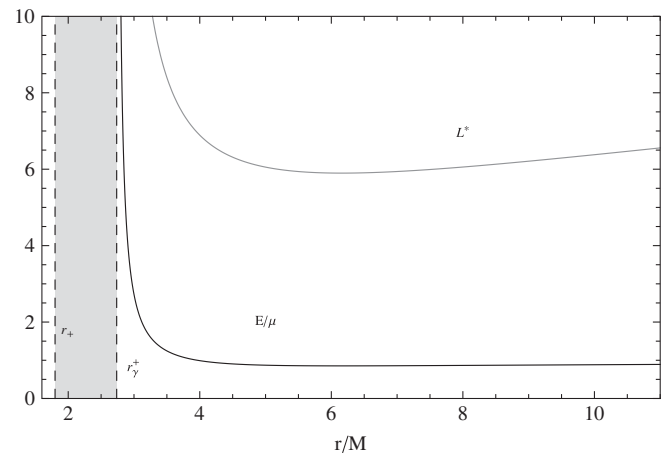


FIG. 7. The energy E/μ and angular momentum $L^* \equiv L/(\mu M)$ of a charged particle of charge-to-mass ratio ϵ moving in the field of a RN black hole with charge Q and mass M are plotted as functions of the radial distance r/M for the parameter choice $Q/M = 0.6$ and $\epsilon = -3$, with $r_\gamma^+/M \approx 2.74$ and the outer horizon located at $r_+/M = 1.8$. The shaded region is forbidden.

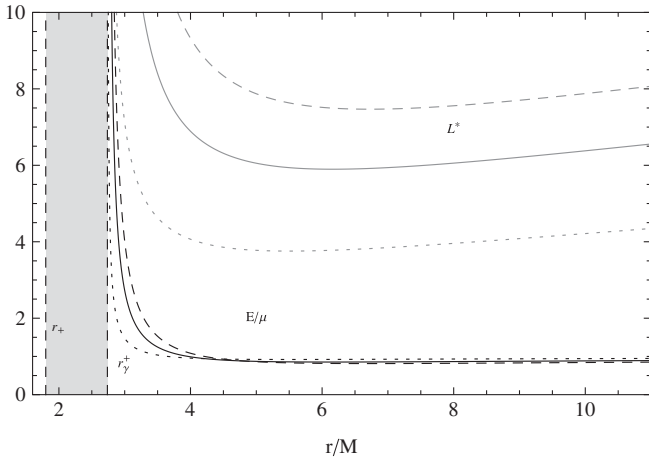


FIG. 8. The energy E/μ and angular momentum $L^* \equiv L/(\mu M)$ of a charged particle of charge-to-mass ratio ϵ moving in the field of a RN black hole with charge Q and mass M are plotted as functions of the radial distance r/M for the parameter choice $Q/M=0.6$ and $\epsilon = -3$ (solid curves), $\epsilon = -5$ (dashed curves), $\epsilon = -0.5$ (dotted curves). Here $r_\gamma^+/M \approx 2.74$ and the outer horizon is located at $r_+/M = 1.8$. The shaded region is forbidden. The energy and angular momentum decrease as $|\epsilon|$ decreases.

the region $r > r_\gamma^+$, the orbital velocity increases as the radius approaches the value r_γ^+ (see Fig. 9). The interval $r_l \leq r \leq r_\gamma^+$ presents a much more complex dynamical structure. First we note that, due to the Coulomb repulsive force, charged particle orbits are allowed in a region which is forbidden for neutral test particles. This is an interesting result leading to the possibility of accretion disks in which the innermost part forms a ring of charged particles only. Indeed, suppose that an accretion disk around a

RN black hole is made of neutral and charged test particles. Then, the accretion disk can exist only in the region $r \geq r_l$ with a ring of charged particles in the interval $[r_l, r_\gamma^+)$. Outside the exterior radius of the ring ($r > r_\gamma^+$), the disk can be composed of neutral and charged particles. This situation can also be read from Fig. 10 where the energy and the angular momentum are plotted as functions of the radial distance r/M .

(b) $M/Q < \epsilon < \bar{\epsilon}$ and $r_l \leq r \leq r_s$.

Since $r < r_s$, one has that $\epsilon/\epsilon_0 < 1$, implying that both solutions ν_ϵ^+ and ν_ϵ^- can exist. There are two different branches for both signs: $\nu = \pm \nu_\epsilon^+$ in the range $r_l \leq r \leq r_\gamma^+$, and ν_ϵ^- in the entire range $r_l \leq r \leq r_s$. The two branches join at $r = r_l$. Note that for increasing values of ϵ , the radius r_s decreases and approaches r_l , reaching it at $\epsilon = \bar{\epsilon}$, and as ϵ tends to infinity r_s tends to the outer horizon r_+ (see Fig. 11). In particular, the interaction between the attractive gravitational force and the Coulomb force generates a zone $r_l \leq r \leq r_\gamma^+$ in which only charged test particles can move along circular trajectories while neutral particles are allowed in the region $r > r_\gamma^+$ (see Fig. 12). This result again could be used to construct around black holes accretion disks with rings made of charged particles.

(c) $\bar{\epsilon} < \epsilon < \epsilon_l$ and $r_s < r < r_\gamma^+$.

The solution ν_ϵ^- for the linear velocity is not allowed whereas the solution ν_ϵ^+ is valid in the entire range. In fact, the condition $r > r_s$ implies that $\epsilon/\epsilon_0 > 1$, and therefore $\Lambda^2 - 1 + (\epsilon/\epsilon_0)^2 > \Lambda^2$, so that the condition (38) for the existence of velocities is satisfied for the plus sign only. Therefore, the solutions are given by $\nu = \pm \nu_\epsilon^+$ in the entire range as shown in Fig. 13. At the radius orbit $r = r_s$, the

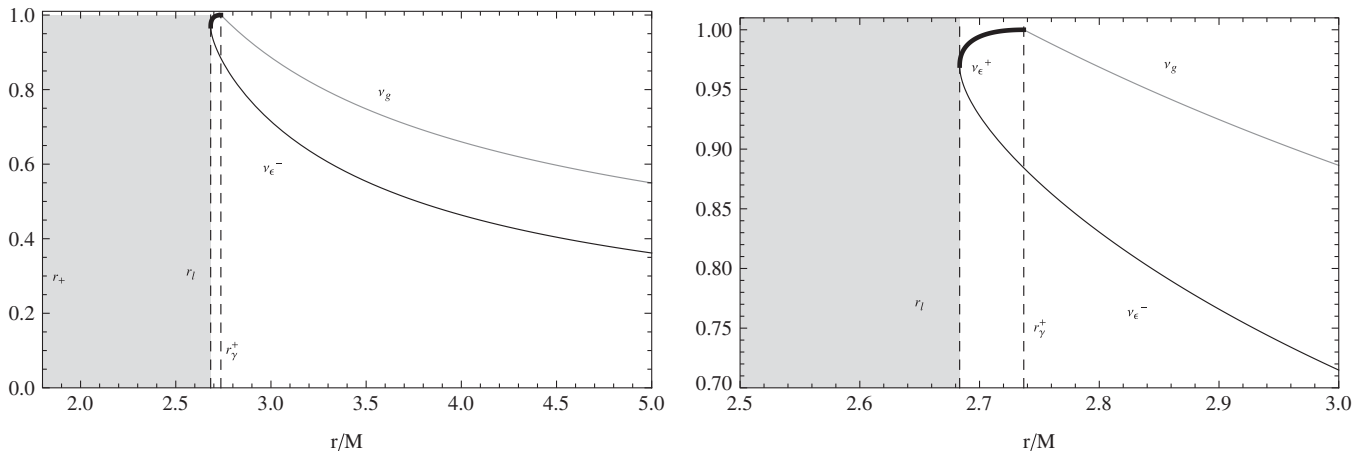


FIG. 9. The positive solution of the linear velocity ν_ϵ^+ is plotted as a function of the radial distance r/M in the region $[1.8, 5]$ (left graphic) and $[2.5, 3]$ (right graphic). Here $Q/M = 0.6$ and $\epsilon = 1.2$, so that $r_l/M = 2.68$ and $r_\gamma^+ = 2.737M$. For the chosen parameters we have that $\bar{\epsilon} = 3.25$ and $\epsilon_l = 4.12$. The region within the interval $[r_l, r_\gamma^+]$ is forbidden for neutral particles.

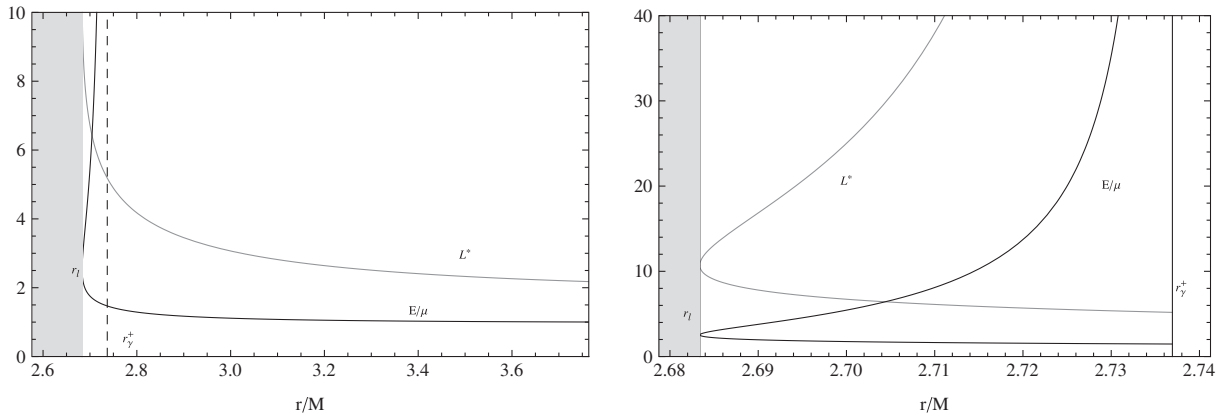


FIG. 10. The energy E/μ and angular momentum $L^* \equiv L/(\mu M)$ of a charged particle of charge-to-mass ratio ϵ moving along circular orbits in a Reissner–Nordström black hole of charge Q and mass M are plotted in terms of the radial distance r/M in the range [2.6, 3.8] (left graphic) [2.68, 2.74] (right graphic). Here $Q/M = 0.6$ and $\epsilon = 1.2$, so that $r_l/M = 2.68$ and $r_\gamma^+/M = 2.737$. For the chosen parameters we have that $\tilde{\epsilon} = 3.25$ $\epsilon_l = 4.12$. The shaded region is forbidden for any particles.

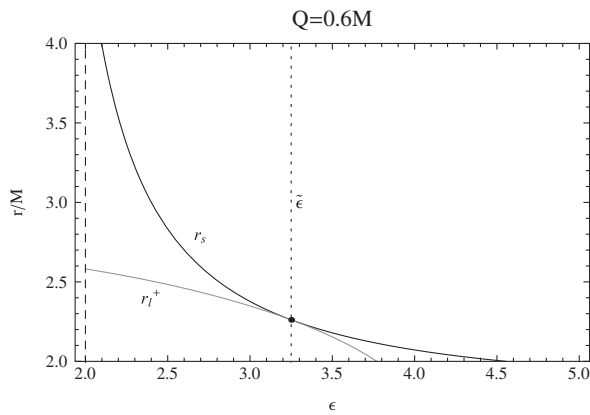


FIG. 11. Radius $r_s = r_s^+$ (black curve) and $r_l = r_l^+$ (gray curve), are plotted as function of ϵ for $Q = 0.6M$. $r_s^+ = r_l^+$ for $\epsilon = \tilde{\epsilon} \approx 3.25$.

angular momentum and the velocity of the test particle vanish, indicating that the particle remains at rest with respect to static observers located at infinity. In the region $r_s < r < r_\gamma^+$ only charged particles can move along circular trajectories.

(d) $\epsilon > \epsilon_l$ and $r_s < r < r_\gamma^+$.

In this case the radius r_l does not exist. The solutions are the velocities $\nu = \pm \nu_\epsilon^+$ in the entire range. Note that for $\epsilon \rightarrow \infty$ one has that $r_s \rightarrow r_+$. Also in this case we note that neutral particles can stay in circular orbits with a velocity ν_g only in the region $r > r_\gamma^+$ whereas charged test particles are allowed within the interval $r_s < r < r_\gamma^+$, as shown in Fig. 14. Clearly, for charged and neutral test particles the circular orbit at $r = r_\gamma^+$ corresponds to a limiting orbit.

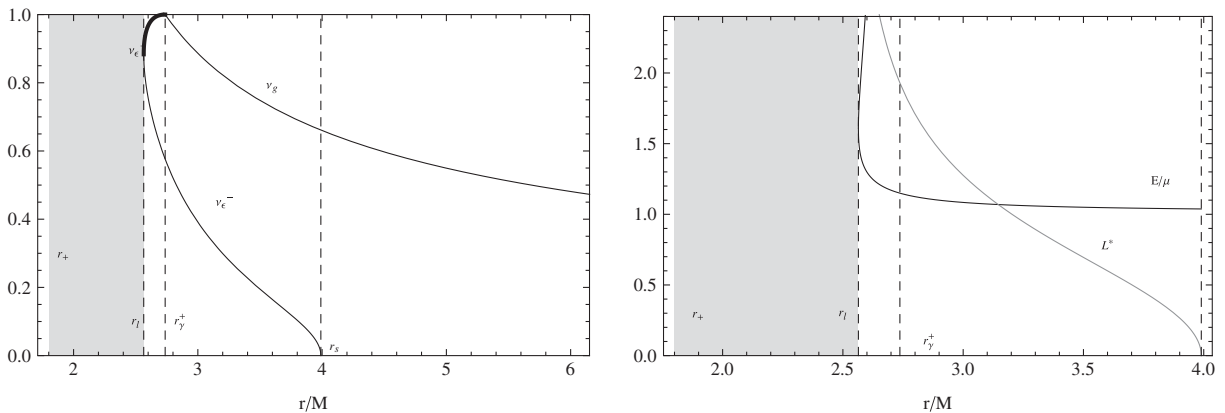


FIG. 12. Left graphic: The positive solution of the linear velocity ν is plotted as a function of the radial distance r/M . Right graphic: The energy E/μ and angular momentum $L^* \equiv L/(\mu M)$ of a charged particle of charge-to-mass ratio ϵ are plotted in terms of r/M . The parameter choice is $Q/M = 0.6$ and $\epsilon = 2.1$. Then, $r_l/M = 2.56$, $r_\gamma^+/M = 2.737$, and $r_s/M = 3.99$. Moreover, for this choice $\tilde{\epsilon} = 3.25$ and $\epsilon_l = 4.12$. The shaded region is forbidden.

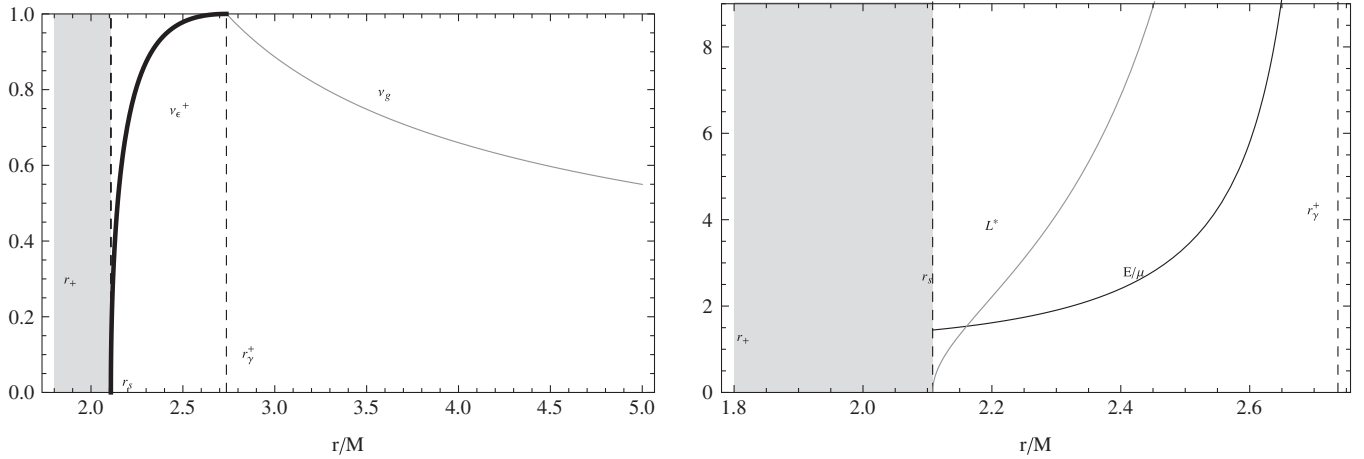


FIG. 13. Left graphic: The positive solution of the linear velocity ν is plotted as a function of the radial distance r/M . Right graphic: The energy E/μ and angular momentum $L^* \equiv L/(\mu M)$ of a charged particle of charge-to-mass ratio $\epsilon = 3.8$ moving in a RN spacetime with $Q/M = 0.6$ are plotted in terms of the radial distance r/M . For this choice of parameters the radii are $r_+/M = 1.98$, $r_s/M = 2.11$, and $r_\gamma^+/M = 2.737$ whereas the charge parameters are $\tilde{\epsilon} = 3.25$ and $\epsilon_l = 4.12$.

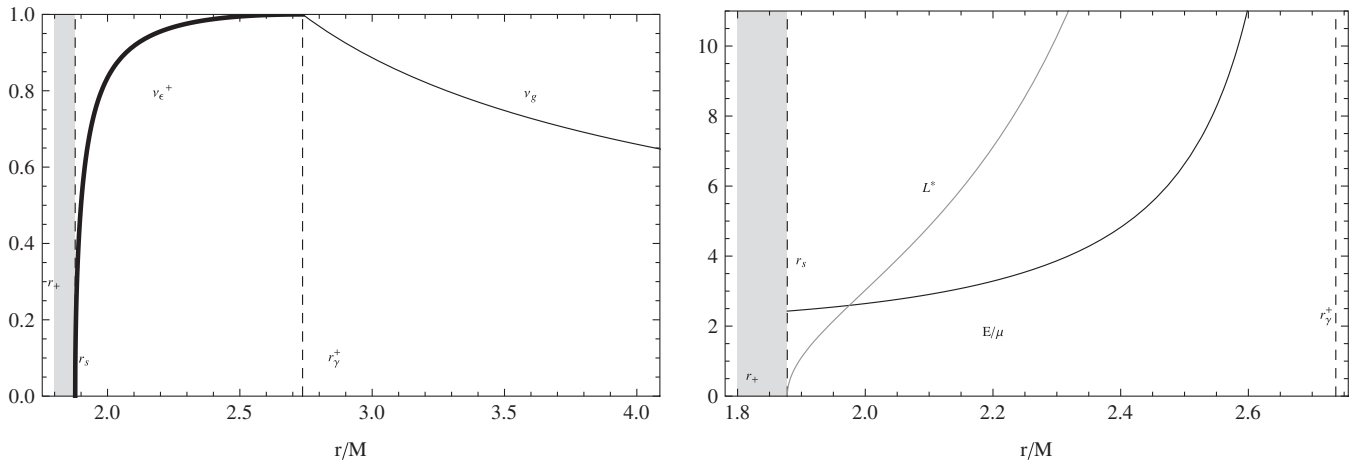


FIG. 14. Left graphic: The positive solution of the linear velocity ν is plotted as a function of the radial distance r/M . Right graphic: The energy E/μ and angular momentum $L^* \equiv L/(\mu M)$ of a charged particle of charge-to-mass ratio $\epsilon = 7$, moving in the field of a RN black hole with $Q/M = 0.6$, are plotted in terms of the radial distance r/M . For this parameter choice $r_s/M = 1.88$, $\tilde{\epsilon} = 3.25$, and $\epsilon_l = 4.12$.

Stability

To analyze the stability of circular orbits for charged test particles in a RN black hole we must consider the condition (16) which leads to the Eqs. (17) and (18). So, the stability of circular orbits strongly depends on the sign of (ϵQ) . The case $\epsilon Q \leq 0$ is illustrated in Fig. 15, where the radius of the last stable circular orbit r_{lsc0} is plotted for two different values of ϵ as a function of Q/M . It can be seen that the energy and angular momentum of the particles decrease as the value of Q/M increases. These graphics also include the radius of the outer horizon r_+ and the radius r_γ^+ which determines the last (unstable) circular orbit of neutral particles. In Sec. III, we found that circular orbits for charged particles are allowed also inside the radius r_γ^+

for certain values of the parameters; however, since $r_\gamma^+ < r_{\text{lsc0}}$, we conclude that all those orbits must be unstable. From Fig. 16 we see that for $Q = 0$ and $\epsilon = 0$, the well-known result for the Schwarzschild case, $r_{\text{lsc0}} = 6M$, is recovered. Also in the limiting case $Q = M$ and $\epsilon = 0$, we recover the value of $r_{\text{lsc0}} = 4M$ for neutral particles moving along circular orbits in an extreme BN black hole. In general, as the value of $|\epsilon|$ increases, we see that the value of r_{lsc0} increases as well. This behavior resembles the case of the radius of the last stable orbit for neutral test particles [12,13]. Indeed, in the case $\epsilon Q < 0$ the attractive Coulomb force reinforces the attractive gravitational force so that the general structure remains unchanged. We also can expect that an increase in

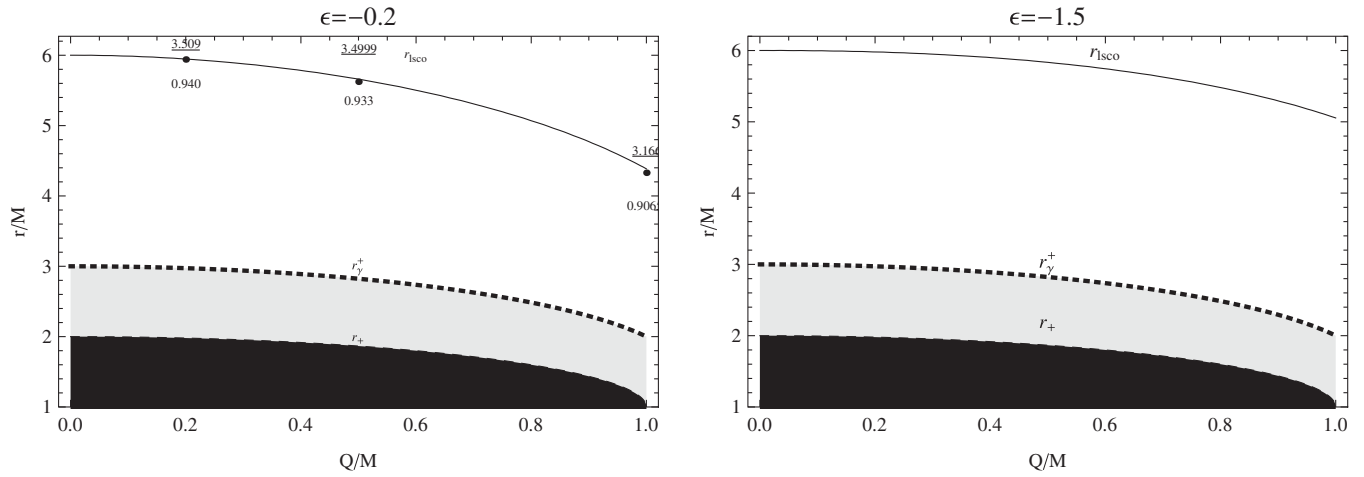


FIG. 15. The radius of the last stable circular orbit r_{lSCO} in a RN black hole of mass M and charge Q for a particle with ratio $\epsilon = -0.2$ (left plot) and $\epsilon = -1.5$ (right plot). Numbers close to the point represent the energy E/μ of the last stable circular orbits at that point. Underlined numbers represent the corresponding angular momentum $L/(M\mu)$. Stable orbits are possible only for $r > r_{\text{lSCO}}$. For comparison we also include the curves for the radii r_+ and r_γ^+ .

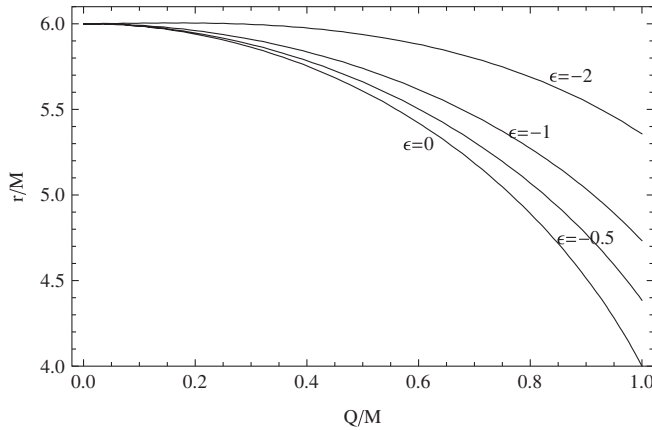


FIG. 16. The radius r_{lSCO} of the last stable circular orbit in a RN black with charge-to-mass ratio Q/M for selected values of the charge-to-mass ratio ϵ of the test particle. Only the case $\epsilon Q \leq 0$ is illustrated. Stable orbits are possible only for $r > r_{\text{lSCO}}$.

the charge of the particle $|\epsilon|$ produces an increase in the velocity of the stable circular orbits. In fact, this can be seen explicitly from Eq. (30) and Fig. 6. It then follows that the energy and angular momentum of the charged test particle increases as the value of $|\epsilon|$ increases.

The case of $\epsilon Q > 0$ is illustrated in Figs. 17 and 18. The situation is very different from the case of neutral particles or charged particles with $\epsilon Q < 0$. Indeed, in this case the Coulomb force is repulsive and leads to a non trivial interaction with the attractive gravitational force, see also [31–40]. It is necessary to analyze two different subcases. The first subcase for $\epsilon > 1$ is illustrated in Fig. 17, while the second one for $0 < \epsilon < 1$ is depicted in Fig. 18. We can see that in the case $0 < \epsilon < 1$ the stability regions

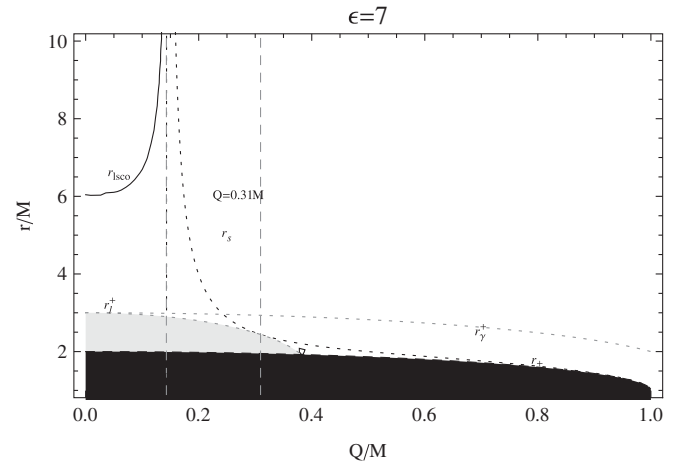


FIG. 17. The radius of the last stable circular orbit r_{lSCO} (solid curve) for a charged test particle with $\epsilon = 7$, in a RN black hole with charge Q and mass M , is plotted as a function of the ratio Q/M . Other curves are the outer horizon radius $r_+ = M + \sqrt{M^2 - Q^2}$ and the radii $r_\gamma^+ \equiv [3M + \sqrt{(9M^2 - 8Q^2)}]/2$, $r_s \equiv \frac{Q^2}{\epsilon^2 Q^2 - M^2} [\epsilon \sqrt{M^2 - Q^2} \sqrt{\epsilon^2 - 1} + M(\epsilon^2 - 1)]$, $r_l \equiv \frac{3M}{2} + \frac{1}{2} \sqrt{9M^2 - 8Q^2 - Q^2 \epsilon^2}$. Shaded and dark regions are forbidden for timelike particles. Stable orbits are possible only for $r > r_{\text{lSCO}}$.

are similar to those found in the case $\epsilon < 0$ (cf. Figs 15 and 18). This means that for weakly-charged test particles, $0 < \epsilon < 1$, it always exists a stable circular orbit and $r_{\text{lSCO}} \geq 4M$, where the equality holds for an extreme black hole. On the contrary, in the case $\epsilon > 1$, there are regions of Q and ϵ in which stable circular orbits cannot exist at all. As can be seen from Fig. 17, charged particles moving along circular orbits with radii located within the region $r < r_\gamma^+$ or $r < r_s$ must be unstable.

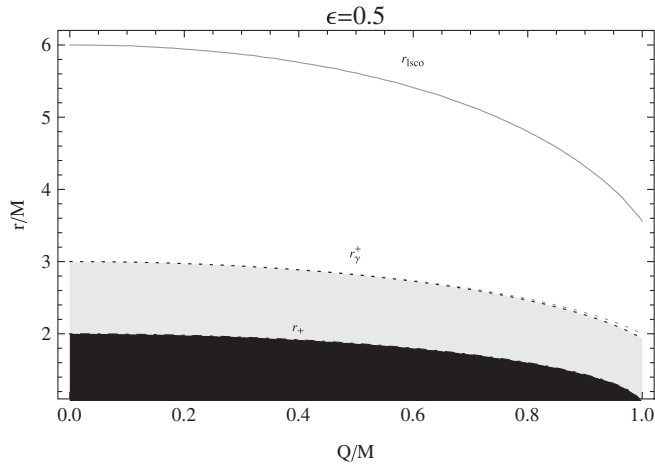


FIG. 18. The radius of the last stable circular orbit r_{lSCO} (solid curve) for a charged test particle with $\epsilon = 0.5$, in a RN black hole with charge Q and mass M , is plotted as a function of the ratio Q/M . Other curves are the outer horizon radius r_+ and the radius r_{γ}^+ . Shaded and dark regions are forbidden for timelike particles. Stable orbits are possible only for $r > r_{\text{lSCO}}$.

We conclude that the ring structure of the hypothetical accretion disks around a RN black hole mentioned in Sec. III must be unstable.

IV. NAKED SINGULARITIES

The effective potential V_{\pm} given in Eq. (9) in the case of naked singularities ($M^2 < Q^2$) is plotted in Figs. 19–22 in terms of the radial coordinate r/M for selected values of the ratio ϵ and the angular momentum $L/(M\mu)$ of the test particle, see also [25,41–47]. The effective potential profile strongly depends on the sign of ϵQ . Moreover, the cases with $|\epsilon| \leq 1$ and with $|\epsilon| > 1$ must be explored separately.

Figure 20 shows the effective potential for a particle of charge-to-mass ϵ in the range $[-10, -1]$. The presence of minima (stable circular orbits) in the effective potential with negative energy states is evident. Moreover, we note that the minimum of each potential decreases as $|\epsilon|$ increases. This fact is due to the attractive and repulsive effects of the gravitational and electric forces [31–40].

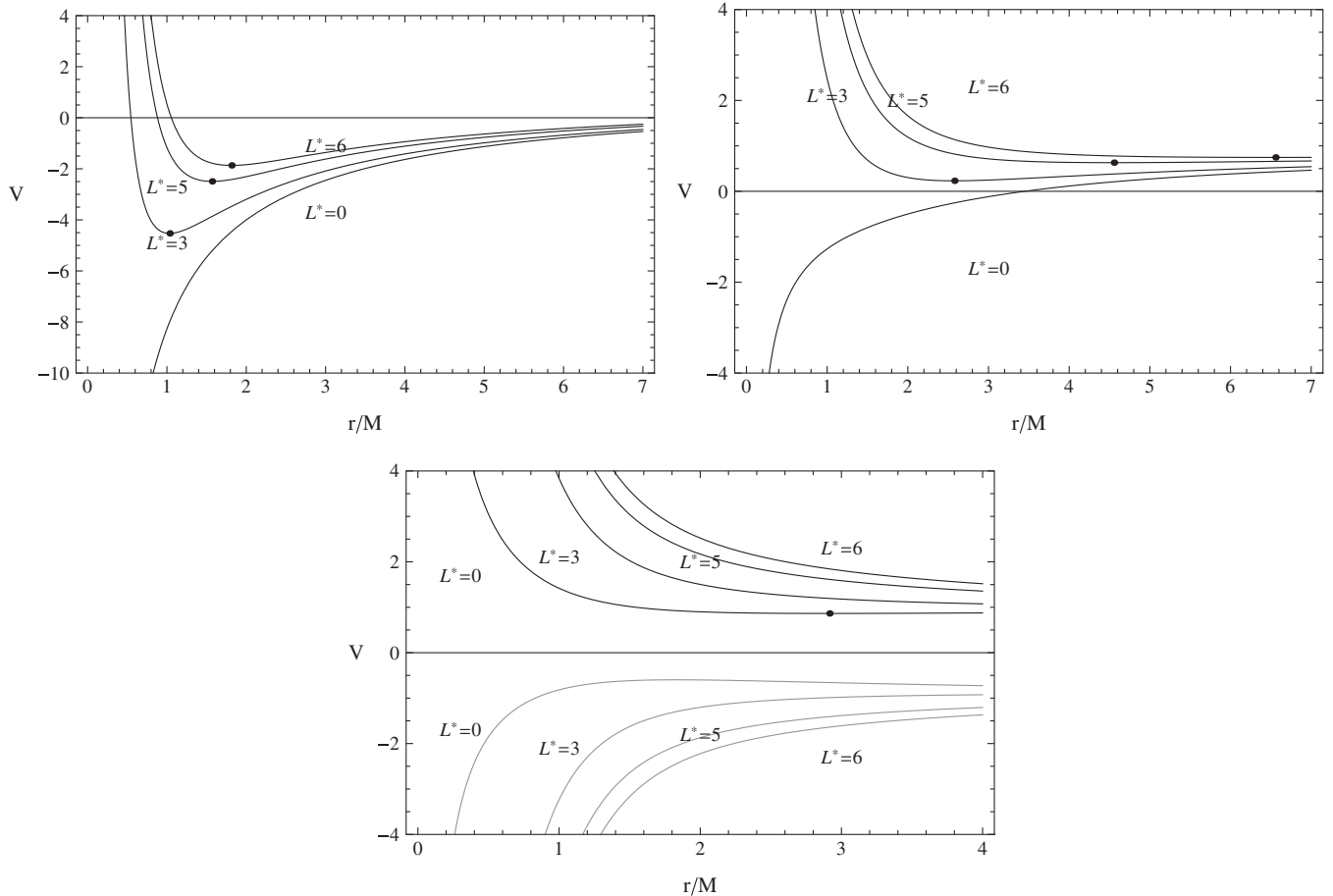


FIG. 19. The effective potential for a charged particle with charge-to-mass ratio ϵ in a RN naked singularity of charge Q and mass M is plotted as a function of the radius r/M for fixed values of the angular momentum $L^* \equiv L/(\mu M)$. Black curves represent the positive solution V_+ while gray curves correspond to V_- . The boldfaced points denote the minima of the potentials. In upper left plot, the parameter choice is $Q/M = 2$ and $\epsilon = -1.5$; the upper right plot is for $Q/M = 2$ and $\epsilon = -5$ while the bottom plot corresponds to the choice $Q/M = 1.5$ and $\epsilon = -0.2$.

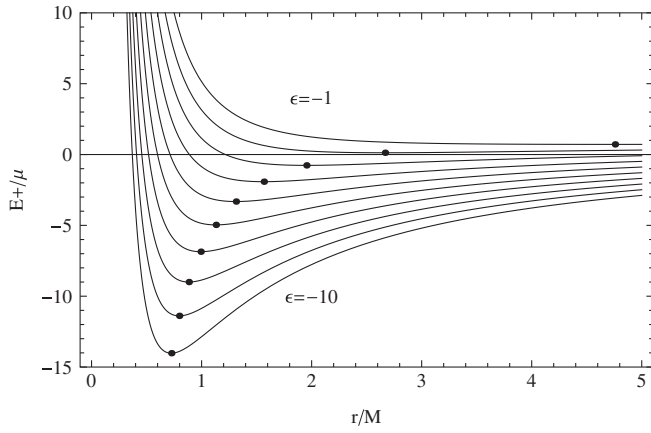


FIG. 20. The effective potential of a RN naked singularity with $Q/M = 2$ for a particle with charge-to-mass ratio ϵ in the range $[-10, -1]$ and angular momentum $L/(M\mu) = 4$.

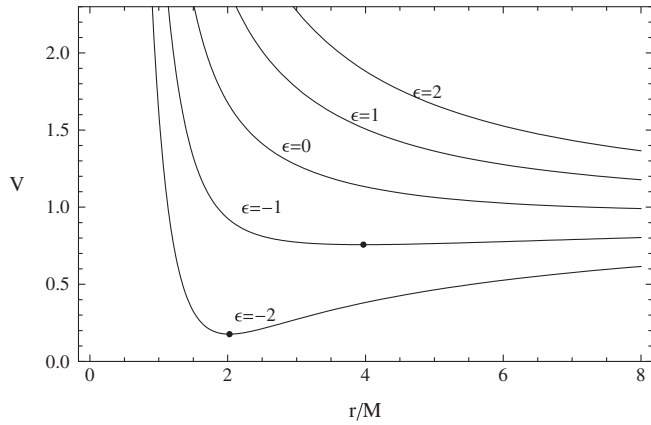
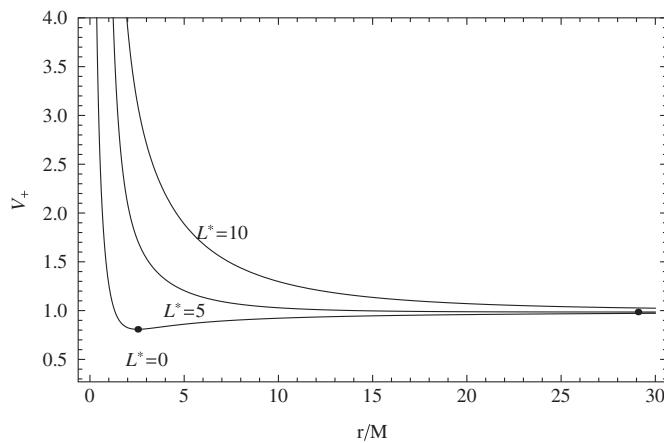


FIG. 21. The effective potential of a RN naked singularity with $Q/M = 3/2$ for a particle with charge-to-mass ratio ϵ in the range $[-2, +2]$ and angular momentum $L/(M\mu) = 4$.



In Fig. 21 the effective potential is plotted for negative and positive values of the charge-to-mass ratio ϵ . We see that for a fixed value of the radial coordinate and the angular momentum of the particle, the value of the potential V increases as the value of ϵ increases. In Fig. 22 we plot the effective potential for a fixed Q/M as function of the radial coordinate and the angular momentum for two different cases, $\epsilon = 0.1$ and $\epsilon = -0.1$. We can see that in the first case the presence of a repulsive Coulomb force reduces the value of the radius of the last stable circular orbit for a fixed angular momentum. We note the existence of stable “circular” orbits with $L = 0$ at which the particle is at rest with respect to static observers located at infinity.

Negative energy states are possible only in the case $\epsilon Q < 0$. The region in which the solution V_+ has negative energy states is

$$0 < r < M + \sqrt{M^2 - Q^2(1 - \epsilon^2)} \quad \text{for } \epsilon \leq -1, \quad (49)$$

and

$$0 < r < r_l^+ \quad \text{for } 0 \leq L < L_q, \quad \epsilon \leq -1, \quad (50)$$

$$r_l^- < r < r_l^+ \quad \text{for } 0 \leq L < L_q, \quad -1 < \epsilon \leq -\sqrt{1 - \frac{M^2}{Q^2}}, \quad (51)$$

where

$$\frac{L_q}{\mu} \equiv r \sqrt{\frac{\epsilon^2 Q^2}{r^2 - 2Mr + Q^2} - 1}. \quad (52)$$

In general, for a particle in circular motion with radius r_0 and charge-to-mass ratio ϵ , around a RN naked singularity with charge Q and mass M , the corresponding angular momentum must be chosen as

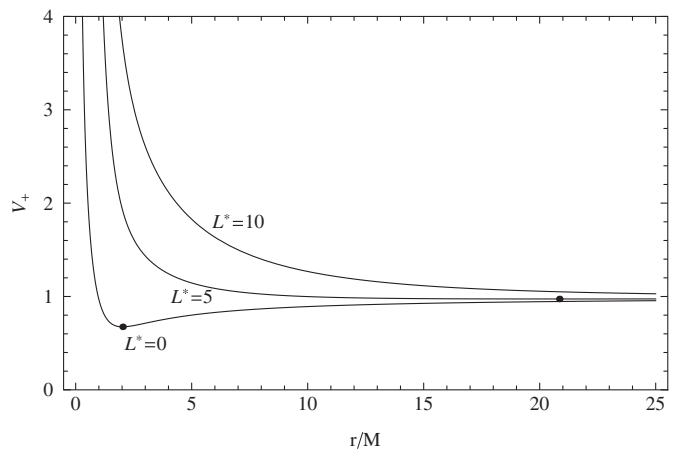


FIG. 22. The effective potential V_+ of a RN naked singularity with $Q/M = 3/2$ for a charged particle is plotted for different values of the angular momentum $L^* \equiv L/(M\mu)$. The left plot corresponds to the ratio $\epsilon = 0.1$ while the right one is for $\epsilon = -0.1$. For $\epsilon = 0.1$ there is a minimum, $V_{\min} \approx 0.81$, at $r_{\min} \approx 2.52M$ for $L^* = 0$, and a minimum, $V_{\min} \approx 0.96$, at $r_{\min} \approx 29M$ for $L^* = 5$. For $\epsilon = -0.1$ the minimum, $V_{\min} \approx 0.67$, is located at $r_{\min} \approx 2.02M$ for $L^* = 0$, and at $r_{\min} \approx 20.8M$ with $V_{\min} \approx 0.97$ for $L^* = 5$.

$$\frac{L^2}{\mu^2} < r_0^2 \left(\frac{\epsilon^2 Q^2}{r_0^2 - 2Mr_0 + Q^2} - 1 \right), \quad (53)$$

in order for negative energy states to exist.

The conditions for circular motion around a RN naked singularity are determined by Eq. (10) which can be used to find the energy and angular momentum of the test particle. Indeed, Eqs. (11) and (12) define the angular momentum L^\pm and the energy E^\pm , respectively, in terms of r/M , Q/M , and ϵ . The explicit dependence of these parameters makes it necessary to investigate several intervals of values. To this end, it is useful to introduce the following notation

$$r_l^\pm \equiv \frac{3M}{2} \pm \frac{1}{2} \sqrt{9M^2 - 8Q^2 - Q^2 \epsilon^2}, \quad (54)$$

$$\tilde{\epsilon}_\pm \equiv \frac{1}{\sqrt{2}Q} \sqrt{5M^2 \pm 4Q^2 + \sqrt{25M^2 - 24Q^2}}, \quad (55)$$

and

$$\tilde{\tilde{\epsilon}}_\pm \equiv \frac{1}{\sqrt{2}Q} \sqrt{3M^2 - 2Q^2 \pm M \sqrt{9M^2 - 8Q^2}}. \quad (56)$$

We note that

$$\lim_{\epsilon \rightarrow 0} r_s^\pm = r_* = \frac{Q^2}{M}, \quad (57)$$

which corresponds to the classical radius of a mass M with charge Q , see for example [48,49], and

$$\lim_{\epsilon \rightarrow 0} r_l^\pm = r_\gamma^\pm = \frac{3M}{2} \pm \frac{1}{2} \sqrt{9M^2 - 8Q^2}, \quad (58)$$

which represents the limiting radius at which neutral particles can be in circular motion around a RN naked singularity [12].

The behavior of the charge parameters defined above is depicted in Fig. 23 in terms of the ratio $Q/M > 1$. It follows from Fig. 23 that it is necessary to consider the following intervals:

$$Q/M \in (1, 5/(2\sqrt{6})], \quad (59)$$

$$Q/M \in (5/(2\sqrt{6}), (3\sqrt{6})/7], \quad (60)$$

$$Q/M \in ((3\sqrt{6})/7, \sqrt{9/8}], \quad (61)$$

$$Q/M \in [\sqrt{9/8}, \infty). \quad (62)$$

Our approach consists in analyzing the conditions for the existence of circular orbits by using the expressions for the angular momentum, Eq. (11), and the energy, Eq. (12), of the particle together with the expressions for the velocity obtained in Sec. III. We consider separately the case $\epsilon > 0$ in Secs. IV A and IV B, and $\epsilon < 0$ in Secs. IV C and IV D.

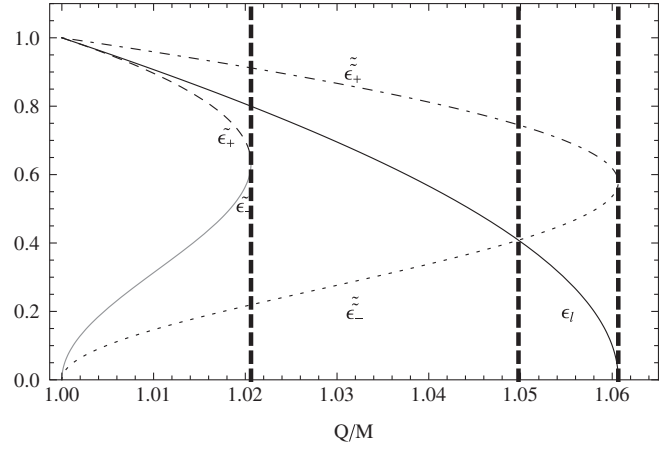


FIG. 23. The charge parameters ϵ_l (black solid curve), $\tilde{\epsilon}_-$ (gray solid curve), $\tilde{\epsilon}_+$ (dashed curve), $\tilde{\tilde{\epsilon}}_-$ (dotted curve), and $\tilde{\tilde{\epsilon}}_+$ (dot-dashed curve) as functions of the charge-to-mass ratio of the RN naked singularity. The special lines $Q/M = 5/(2\sqrt{6}) \approx 1.02$, $Q/M = 3\sqrt{6}/7 \approx 1.05$, and $Q/M = \sqrt{9/8} \approx 1.06$ are also plotted.

In the Appendix, we present equivalent results by using the alternative method of the proper linear velocity of test particles in an orthonormal frame as formulated in Sec. III.

A. Case $\epsilon > 1$

For $\epsilon > 0$, the condition (33) implies in general that $r > r_* \equiv Q^2/M$. Imposing this constraint on Eqs. (11) and (12), we obtain the following results for timelike orbits. For $\epsilon > 1$ and $M < Q < \sqrt{9/8}M$ circular orbits exist with angular momentum $L = L^+$ in the interval $r_\gamma^- < r < r_\gamma^+$, while for $Q \geq \sqrt{9/8}M$ no circular orbits exist (see Fig. 24).

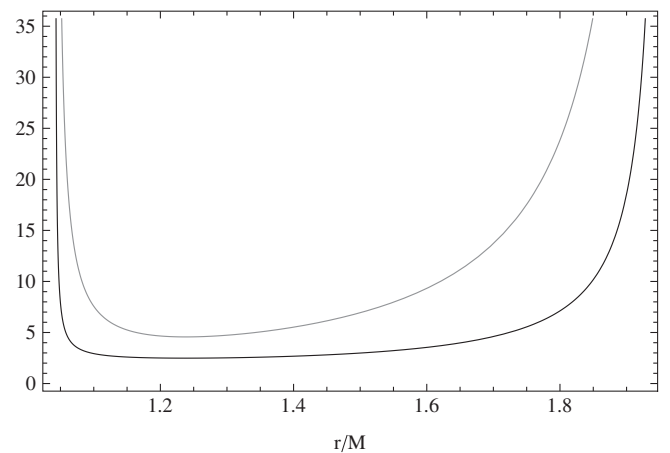


FIG. 24. The case $\epsilon > 1$. The energy (black curve) and angular momentum (gray curve) for a test particle with charge-to-mass ratio $\epsilon = 2$ in a RN naked singularity with $Q = 1.06M$. Circular orbits exist in the interval $r_\gamma^- < r < r_\gamma^+$, where $r_\gamma^- = 1.04196M$ and $r_\gamma^+ = 1.95804M$.

Clearly, the energy and angular momentum of circular orbits diverge as r approaches the limiting orbits at r_γ^\pm . This means that charged test particles located in the region $r_\gamma^- < r < r_\gamma^+$ need to acquire an infinite amount of energy to reach the orbits at r_γ^\pm . The energy of the states is always positive. A hypothetical accretion disk would consist in this case of a charged ring of inner radius r_γ^- and outer radius r_γ^+ , surrounded by a disk of neutral particles. The boundary $r = r_\gamma^+$ in this case would be a lightlike hypersurface.

Since for $\epsilon Q > 0$ the Coulomb interaction is repulsive, the situation characterized by the values for $Q \geq \sqrt{9/8}M$ and $\epsilon > 1$ corresponds to a repulsive electromagnetic effect that cannot be balanced by the attractive gravitational interaction. We note that the case $Q \geq \sqrt{9/8}M$ and $\epsilon > 1$ could be associated to the realistic configuration of a positive ion or a positron in the background of a RN naked singularity.

B. Case $0 < \epsilon < 1$

It turns out that in this case it is necessary to consider separately each of the four different regions for the ratio Q/M that follow from Fig. 23. Moreover, in each region of Q/M it is also necessary to consider the value of ϵ for each of the zones determined by the charge parameters ϵ_l , $\tilde{\epsilon}_\pm$, and $\tilde{\epsilon}_\pm$, as shown in Fig. 23. We analyzed all the resulting cases in detail and found the values of the energy and angular momentum of charged test particles in all the intervals where circular motion is allowed. We summarize the results as follows.

There is always a minimum radius r_{\min} at which circular motion is allowed. We found that either $r_{\min} = r_s^+$ or $r_{\min} = r_\gamma^-$. Usually, at the radius r_s^+ the test particle acquires a zero angular momentum so that a static observer at infinity would consider the particle as being at rest. Furthermore, at the radius r_γ^- the energy of the test particle diverges, indicating that the hypersurface $r = r_\gamma^-$ is

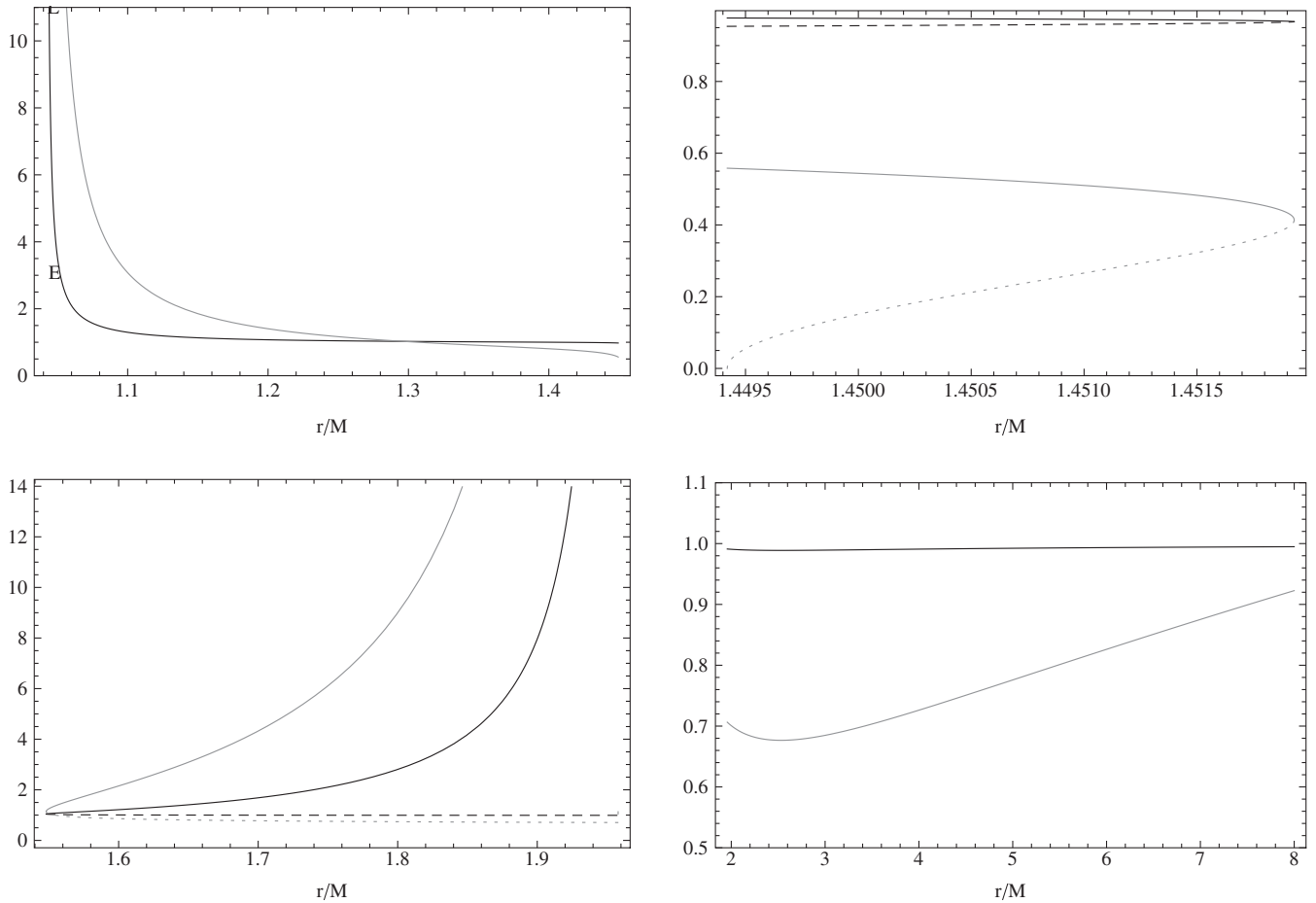


FIG. 25. Case: $M < Q \leq 5/(2\sqrt{6})M$ and $\tilde{\epsilon}_+ < \epsilon \leq \epsilon_l$. Parameter choice: $Q = 1.01M$ and $\epsilon = 0.902$. Then $\epsilon_l = 0.907$, $\tilde{\epsilon}_+ = 0.8963$, $r_s^+ = 1.44942M$, $r_\gamma^- = 1.04196M$, $r_\gamma^+ = 1.95804M$, $r_l^- = 1.45192M$, and $r_l^+ = 1.548077M$. Circular orbits exist with angular momentum $L = L^+$ (gray curves) and energy $E = E^+$ (black curves) in $r_\gamma^- < r < r_s^+$ (upper left plot); $L = L^\pm$ in $r_s^+ \leq r < r_l^-$ (upper right plot) and $r_l^+ \leq r < r_\gamma^+$ (bottom left plot); $L = L^-$ in $r \geq r_\gamma^+$ (bottom right plot).

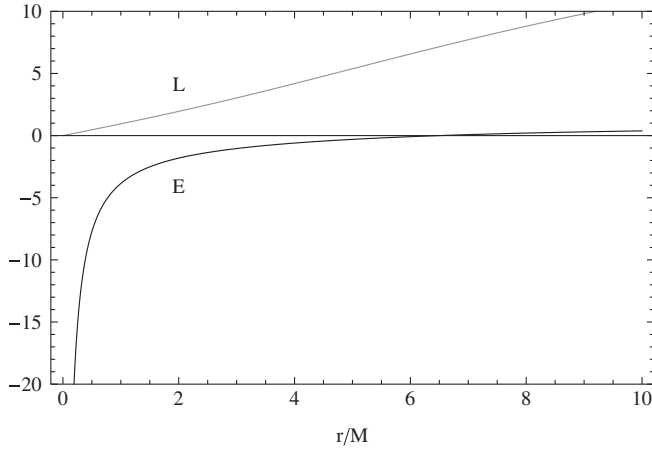


FIG. 26. Case: $\epsilon < -1$ and $Q > \sqrt{9/8}M$. Parameter choice: $Q = 2M$ and $\epsilon = -2$. Circular orbits exist with angular momentum $L = L^+$ (gray curve) and energy $E = E^+$ (black curve).

lightlike. In the simplest case, circular orbits are allowed in the infinite interval $[r_{\min}, \infty)$ so that, at any given radius greater than r_{\min} , it is always possible to have a charged test particle moving on a circular trajectory. Sometimes, inside the infinite interval $[r_{\min}, \infty)$, there exists a lightlike hypersurface situated at $r_{\gamma}^+ > r_{\min}$.

Another possible structure is that of a finite region filled with charged particles within the spatial interval $(r_{\min} = r_{\gamma}^-, r_{\max} = r_{\gamma}^+)$. This region is usually surrounded by an empty finite region in which no motion is allowed. Outside the empty region, we find a zone of allowed circular motion in which either only neutral particles or neutral and charged particles can exist in circular motion. Clearly, this spatial configuration formed by two separated regions in which circular motion is allowed, could be used to build with test particles an accretion disk of disconnected rings. A particular example of this case is illustrated in Fig. 25.

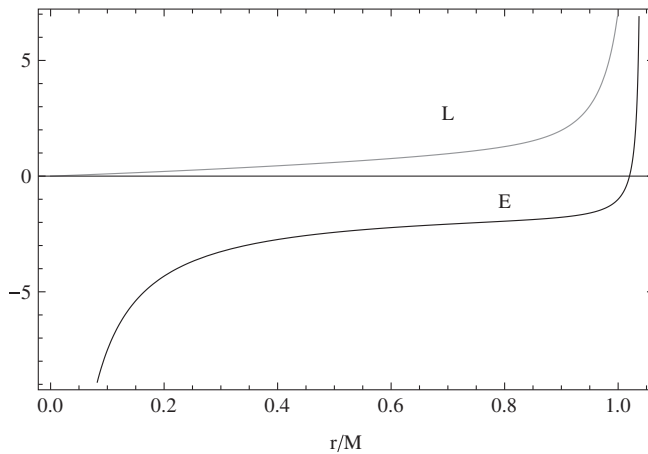


FIG. 27. Case: $\epsilon < -1$ and $M < Q \leq \sqrt{9/8}M$. Parameter choice: $Q = 1.01M$ and $\epsilon = -2$. Then, $r_{\gamma}^- = 1.04196M$ and $r_{\gamma}^+ = 1.95804M$. Circular orbits exist with angular momentum $L = L^+$ (gray curve) and energy $E = E^+$ (black curve) in $0 < r < r_{\gamma}^-$ and $r > r_{\gamma}^+$.

C. Case $\epsilon < -1$

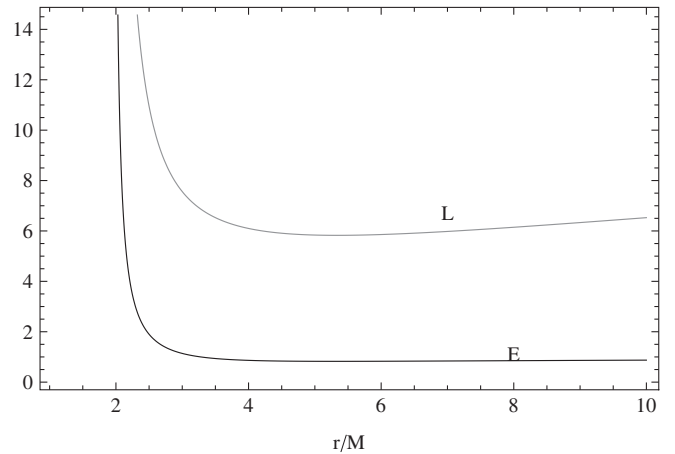
The contribution of the electromagnetic interaction in this case is always attractive. Hence, the only repulsive force to balance the attractive effects of the gravitational and Coulomb interactions can be generated only by the RN naked singularity. This case therefore can be compared with the neutral test particle motion as studied in [12,13]. Then, it is convenient, as in the case of a neutral test particle, to consider the two regions $Q > \sqrt{9/8}M$ and $M < Q \leq \sqrt{9/8}M$ separately.

For $\epsilon < -1$ and for $Q > \sqrt{9/8}M$ circular orbits with $L = L^+$ always exist for $r > 0$ (in fact, however, one has to consider also the limit $r > r_*$ for the existence of timelike trajectories). This case is illustrated in Fig. 26 where the presence of orbits with negative energy states is evident.

For $M < Q \leq \sqrt{9/8}M$ circular orbits exist with $L = L^+$ in $0 < r < r_{\gamma}^-$ and $r > r_{\gamma}^+$ (see Fig. 27). We note that for neutral test particles in the region $M < Q \leq \sqrt{9/8}M$, (stable) circular orbits are possible for $r > r_* = Q^2/M$. At $r = r_*$, the angular momentum of the particle vanishes [12]. On the contrary, charged test particles with $\epsilon < -1$ can move along circular orbits also in the region $(0, r_*)$. The value of the energy on circular orbits increases as r approaches $r = 0$. However, the angular momentum, as seen by an observer located at infinity, decreases as the radius of the orbit decreases. In the region $M < Q \leq \sqrt{9/8}M$, two limiting orbits appear at r_{γ}^{\pm} , as in the neutral particle case [12].

D. Case $-1 < \epsilon < 0$

For this range of the ratio ϵ , it is also convenient to analyze separately the two cases $Q > \sqrt{9/8}M$ and $M < Q \leq \sqrt{9/8}M$. In each case, it is necessary to analyze the explicit value of ϵ with respect to the ratio M/Q . Several



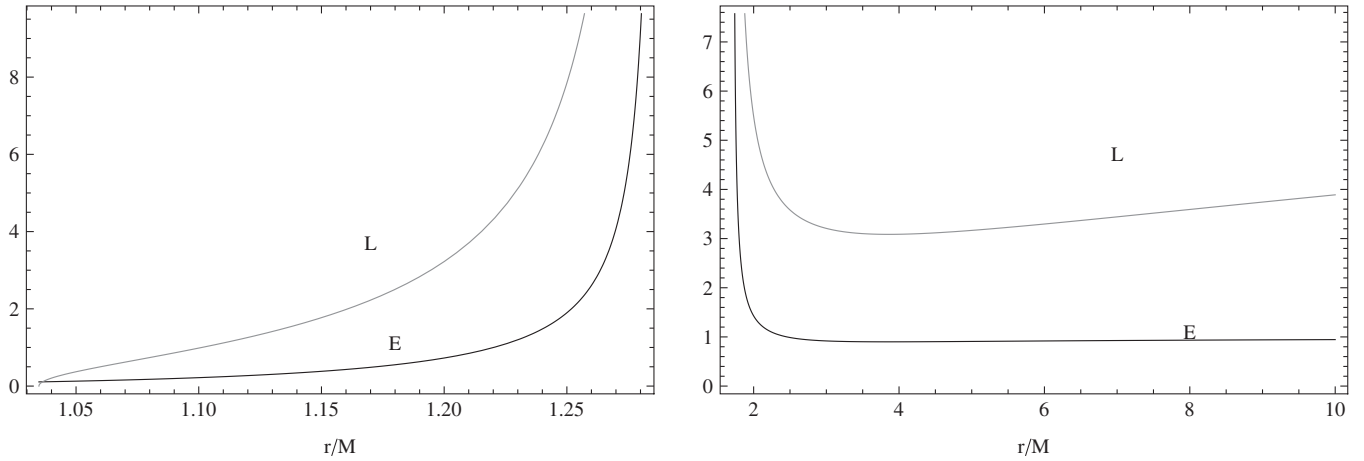


FIG. 28. Case: $M < Q \leq \sqrt{9/8}M$ and $-M/Q < \epsilon < 0$. Parameter choice: $Q = 1.05M$ and $\epsilon = -0.2$. Then $r_\gamma^- = 1.28787M$, $r_\gamma^+ = 1.71213M$, and $r_s^- = 1.03487M$. Circular orbits exist with angular momentum $L = L^+$ (gray curve) and energy $E = E^+$ (black curve) in $r_s^- < r < r_\gamma^-$ (left plot) and in $r > r_\gamma^+$ (right plot). For $r = r_s^-$, $L = 0$.

cases arise in which we must find the regions where circular motion is allowed and the value of the angular momentum and energy of the rotating charged test particles.

We summarize the results in the following manner. There are two different configurations for the regions in which circular motion of charged test particles is allowed. The first one arises in the case $Q > \sqrt{9/8}M$, and consists in a continuous region that extends from a minimum radius r_{\min} to infinity, in principle. The explicit value of the minimum radius depends on the value of ϵ and can be either r_s^- , r_s^+ , or $r_{\min} = Q^2/(2M)$. In general, we find that particles standing on the minimum radius are characterized by $L = 0$, i. e., they are static with respect to a nonrotating observer located at infinity.

The second configuration appears for $M < Q \leq \sqrt{9/8}M$. It also extends from r_{\min} to infinity, but inside it there is a forbidden region delimited by the radii r_γ^- and r_γ^+ . The configuration is therefore composed of two disconnected regions. At the minimum radius, test particles are characterized by $L = 0$. On the boundaries (r_γ^\pm) of the interior forbidden region only photons can stand on circular orbits. A particular example of this case is presented in Fig. 28.

E. Stability

To explore the stability properties of the circular motion of charged test particles in a RN naked singularity, it is necessary to investigate the Eq. (16) or, equivalently, Eqs. (17) and (18), considering the different values for ϵ and $Q/M > 1$. We can distinguish two different cases, $|\epsilon| > 1$ and $0 < |\epsilon| < 1$. Let us consider the case $|\epsilon| > 1$. In particular, as it was shown in Sec. IVA, for $\epsilon > 1$ and $M < Q < \sqrt{9/8}M$ circular orbits exist with $L = L^+$ in the interval $r_\gamma^- < r < r_\gamma^+$ whereas no circular orbits exist for

$\epsilon > 1$ and $Q > \sqrt{9/8}M$. For this particular case, a numerical analysis of condition (16) leads to the conclusion that a circular orbit is stable only if its radius r_0 satisfies the condition $r_0 > r_{\text{lsc0}}$, where r_{lsc0} is depicted in Fig. 29. We see that in general, the radius of the last stable circular orbit is located inside the interval (r_γ^-, r_γ^+) . It then follows that the only stable region is determined by the interval $r_{\text{lsc0}} < r < r_\gamma^+$.

Consider now the case $\epsilon < -1$. The numerical investigation of the condition (16) for the last stable circular orbit shows that in this case, there are two solutions r_{lsc0}^\pm such that $r_{\text{lsc0}}^- \leq r_{\text{lsc0}}^+$, where the equality is valid for

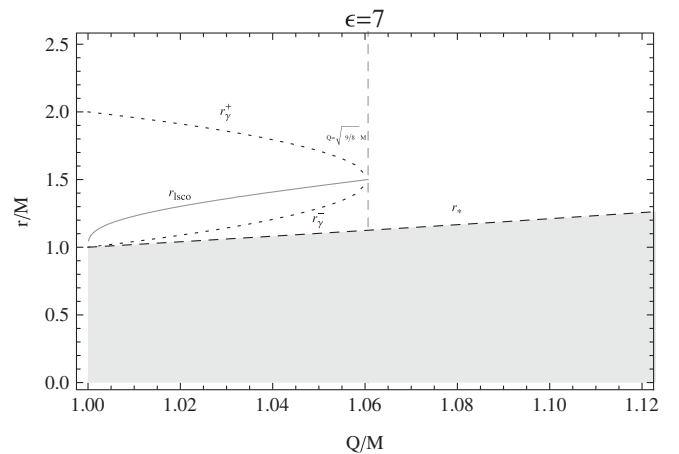


FIG. 29. The radius of the last stable circular orbit r_{lsc0} (gray curve) of a charged particle with ratio $\epsilon = +7$ in a RN naked singularity with ratio $Q/M \in [1, 1.2]$. The radii $r_* = Q^2/M$ and $r = r_\gamma^\pm \equiv [3M \pm \sqrt{9M^2 - 8Q^2}]/2$ are also plotted. Circular orbits exist only in the interval $1 < Q/M < \sqrt{9/8}$. The shaded region is forbidden for timelike particles. Stable orbits are located in the region $r > r_{\text{lsc0}}$.

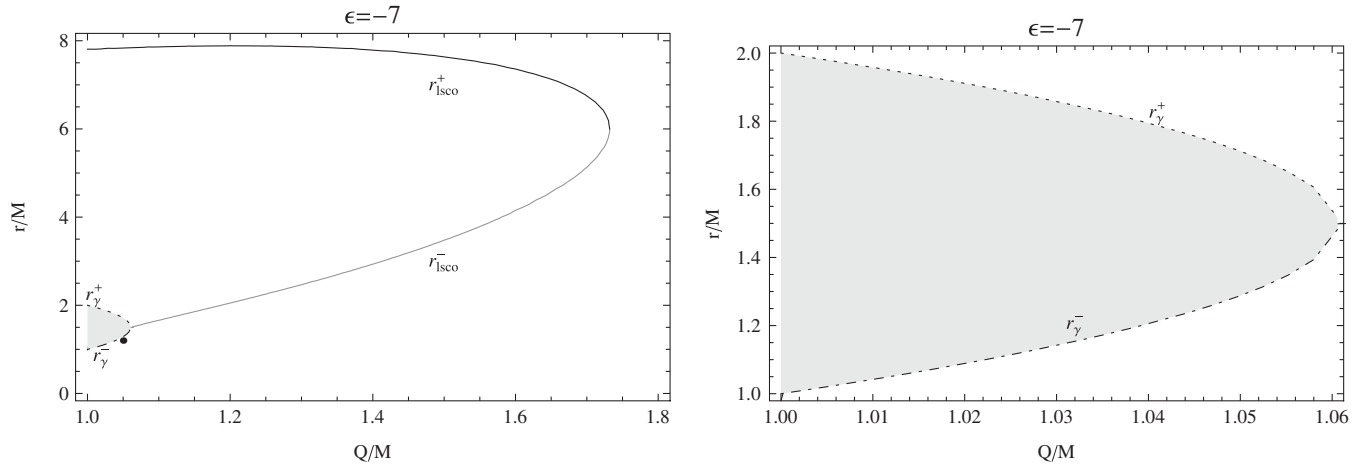


FIG. 30. The radius of the last stable circular orbit r_{lSCO}^{\pm} (black curves) of a charged particle with ratio $\epsilon = -7$ in a RN naked singularity with ratio $Q/M \in [1, 1.8]$. The radii r_* and r_{γ}^{\pm} are also plotted for comparison. In the shaded region no circular orbits can exist. Stable circular orbits are situated outside the region with boundaries r_{lSCO}^+ , r_{lSCO}^- , and the vertical axis $Q/M = 1$.

$Q/M \approx 1.72$. Moreover, for $Q/M = \sqrt{9/8}$ we obtain that $r_{\text{lSCO}}^- = r_{\gamma}^- = r_{\gamma}^+$. This situation is illustrated in Fig. 30. Stable orbits corresponds to points located outside the region delimited by the curves $r = r_{\text{lSCO}}^+$, $r = r_{\text{lSCO}}^-$, and the axis $Q/M = 1$. On the other hand, we found in Sec. IV C that for $\epsilon < -1$ and $1 < Q/M \leq \sqrt{9/8}$ circular orbits exist in the interval $0 < r < r_{\gamma}^-$ and $r > r_{\gamma}^+$. It then follows that the region of stability corresponds in this case to two disconnected zones determined by $0 < r < r_{\gamma}^-$ and $r > r_{\text{lSCO}}^+$. Moreover, we established in Sec. IV C that for

$\epsilon < -1$ and $\sqrt{9/8} < Q/M$, circular orbits always exist for $r > 0$. Consequently, in the interval $\sqrt{9/8} < Q/M \leq 1.72$, the stable circular orbits are located in the two disconnected regions defined by $0 < r < r_{\text{lSCO}}^-$ and $r > r_{\text{lSCO}}^+$. Finally, for $Q/M \geq 1.72$ all the circular orbits are stable (see Fig. 30).

The case $0 < |\epsilon| < 1$ is much more complex, and needs to be described for different subcases following the classification of orbital regions traced in Sec. IV B for the

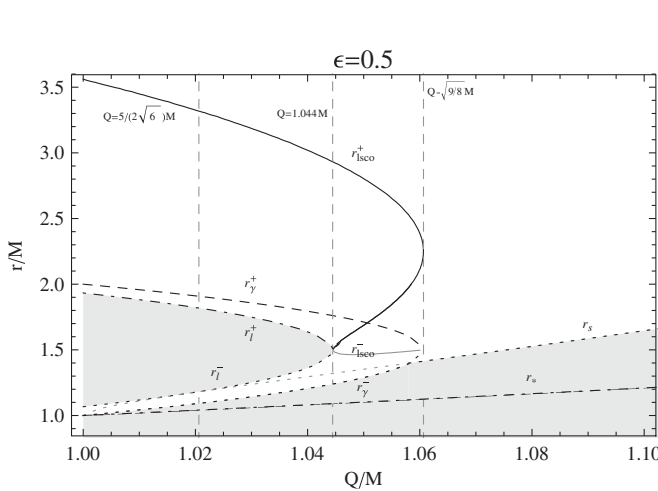


FIG. 31. The radius of the last stable circular orbit r_{lSCO}^{\pm} (black and grey curves) of a charged particle with ratio $\epsilon = 0.5$ in a RN naked singularity with ratio $Q/M \in [1, 1.1]$. Also plotted: $r_{\gamma}^{\pm} \equiv [3M \pm \sqrt{(9M^2 - 8Q^2)}]/2$, $r_s^{\pm} \equiv \frac{Q^2}{\epsilon^2 Q^2 - M^2} [\sqrt{\epsilon^2(\epsilon^2 - 1)(M^2 - Q^2)} \times M(\epsilon^2 - 1)]$, $r_l^{\pm} \equiv \frac{3M}{2} \pm \frac{1}{2} \sqrt{9M^2 - 8Q^2 - Q^2 \epsilon^2}$, and $r_* = Q^2/M$. Regions of stability are: for $Q > \sqrt{9/8}M$ in $r > r_s$, for $(3\sqrt{6}/7)M < Q < \sqrt{9/8}M$ exist stable orbits in $r_{\gamma}^- < r$, for $(5/(2\sqrt{6}))M < Q < (3\sqrt{6}/7)M$ exist stable orbits in $r_{\gamma}^- < r$. For $M < Q < (5/(2\sqrt{6}))M$ stable orbits are located in $r > r_{\text{lSCO}}^+$.

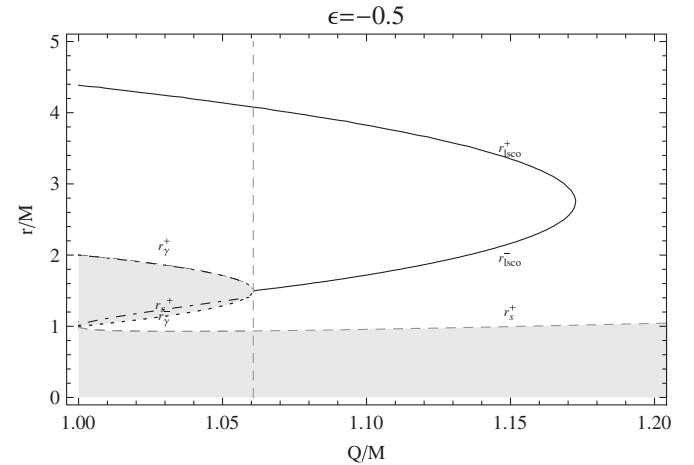


FIG. 32. The radius of the last stable circular orbit r_{lSCO}^{\pm} (black and grey curves) of a charged particle with ratio $\epsilon = -0.5$ in a RN naked singularity with ratio $Q/M \in [1, 1.2]$. Also plotted: $r_{\gamma}^{\pm} \equiv [3M \pm \sqrt{(9M^2 - 8Q^2)}]/2$, $r_s^+ \equiv \frac{Q^2}{\epsilon^2 Q^2 - M^2} [\sqrt{\epsilon^2(\epsilon^2 - 1)(M^2 - Q^2)} M(\epsilon^2 - 1)]$, $r_l^+ \equiv \frac{3M}{2} \pm \frac{1}{2} \times \sqrt{9M^2 - 8Q^2 - Q^2 \epsilon^2}$, and $r_* = Q^2/M$. Shaded regions are forbidden. Regions of stability are: for $Q > (\sqrt{9/8})M$ stable circular orbits exist in $r_s^+ < r < r_{\text{lSCO}}^-$, and $r > r_{\text{lSCO}}^+$. For $M < Q < (\sqrt{9/8})M$ stable circular orbits exist in $r_s^+ < r < r_{\gamma}^-$, and $r > r_{\gamma}^+$.

case $0 < \epsilon < 1$, and in Sec. **IV D** for the case $-1 < \epsilon < 0$. The results for the specific ratio $\epsilon = 0.5$ are given in Fig. 31 and for $\epsilon = -0.5$ in Fig. 32. In general, we find that the results are similar to those obtained for the case $\epsilon < -1$. Indeed, the zone of stability consists of either one connected region or two disconnected regions. The explicit value of the radii that determine the boundaries of the stability regions depend on the particular values of the ratio Q/M .

V. CONCLUSIONS

In this work, we explored the motion of charged test particles along circular orbits in the spacetime described by the Reissner-Nordström (RN) metric. We performed a very detailed discussion of all the regions of the spacetime where circular orbits are allowed, using as parameters the charge-to-mass ratio Q/M of the source of gravity and the charge-to-mass ratio $\epsilon = q/\mu$ of the test particle. Depending on the value of Q/M , two major cases must be considered: The black hole case, $|Q/M| \leq 1$, and the naked singularity case, $|Q/M| > 1$. Moreover, we found out that the two cases $|\epsilon| \leq 1$ and $|\epsilon| > 1$ must also be investigated separately. Whereas the investigation of the motion of charged test particles with $|\epsilon| > 1$ can be carried out in a relatively simple manner, the case with $|\epsilon| \leq 1$ is much more complex, because it is necessary to consider various subcases which depend on the explicit value of ϵ in this interval.

To perform the analysis of circular motion of charged test particles in this gravitational field, we use two different methods. The first one consists in using constants of motion to reduce the equations of motion to a single first-order differential equation for a particle moving in an effective potential. The properties of this effective potential are then used to find the conditions under which circular motion is possible. The second approach uses a local orthonormal frame to introduce a “local proper linear velocity” for the test particle. The conditions for this velocity to be timelike are then used to determine the regions of space where circular orbits are allowed. The results of both methods are equivalent and, in fact, for the sake of simplicity it is sometimes convenient to use a combination of both approaches. In this work, we analyzed in detail the conditions for the existence of circular orbits and found all the solutions for all the regions of space in the case of black holes and naked singularities.

To formulate the main results of this work in a plausible manner, let us suppose that an accretion disk around a RN gravitational source can be made of test particles moving along circular orbits [50]. Then, in the case of black hole we find two different types of accretion disks made of charged test particles. The first type consists of a disk that begins at a minimum radius R and can extend to infinity, in principle. In the second possible configuration, we find a circular ring of charged particles with radii

($r_{\text{int}}, r_{\text{ext}}$), surrounded by the disk, i. e., with $r_{\text{ext}} < R$. For certain choices of the parameter ϵ , the exterior disk might be composed only of neutral particles. A study of the stability of circular orbits shows that the second structure of a ring plus a disk is highly unstable. This means that test particles in stable circular motion around RN black holes can be put together to form only a single disk that can, in principle, extend to infinity.

In the case of RN naked singularities we find the same two types of accretion disks. The explicit values of the radii $r_{\text{min}}, r_{\text{ext}}$, and R depend on the values of the ratios ϵ and Q/M , and differ significantly from the case of black holes. In fact, we find that the case of naked singularities offers a much richer combination of values of the charge-to-mass ratios for which it is possible to find a structure composed of an interior ring plus an exterior disk. A study of the stability of this specific situation shows that for certain quite general combinations of the parameters the configuration is stable. This result implies that test particles in stable circular motion around RN naked singularities can be put together to form either a single disk that can extend, in principle, to infinity or a configuration of an interior ring with an exterior disk. This is the main difference between black holes and naked singularities from the viewpoint of these hypothetical accretion disks made of test particles.

The question arises whether it is possible to generalize these results to the case of more realistic accretion disks around more general gravitational sources, taking into account, for instance, the rotation of the central body [51,52]. It seems reasonable to expect that in the case of Kerr and Kerr-Newman naked singularities, regions can be found where stable circular motion is not allowed so that an accretion disk around such an object would exhibit a discontinuous structure. Indeed, some preliminary calculations of circular geodesics in the field of rotating compact objects support this expectation. Thus, we can conjecture that the discontinuities in the accretion disks around naked singularities are a consequence of the intensity of the repulsive gravity effects that characterize these speculative objects. Furthermore, it was recently proposed that static compact objects with quadrupole moment can be interpreted as describing the exterior gravitational field of naked singularities [53,54]. It would be interesting to test the above conjecture in this relatively simple case in which rotation is absent. If the conjecture turns out to be true, it would give us the possibility of distinguishing between black holes and naked singularities by observing their accretion disks.

ACKNOWLEDGMENTS

Daniela Pugliese and Hernando Quevedo would like to thank the ICRANet for support. We would like to thank Andrea Geralico for helpful comments and discussions. One of us (D. P.) gratefully acknowledges financial support

from the A. Della Riccia Foundation. This work was supported in part by DGAPA-UNAM, grant No. IN106110.

APPENDIX: VELOCITY OF TEST PARTICLES IN A RN NAKED SINGULARITY

In this Appendix we explore charged test particles in circular motion in a RN naked singularity by using the tetrad formalism, as developed in Sec. III for the black hole analysis. In Sec. IV, we studied the timelike circular motion in the naked singularity case by analyzing directly the existence conditions for the energy, Eq. (12), and the angular momentum, Eq. (11). Here, we use the formalism of “local proper linear velocity” as measured by an observer attached to an orthonormal frame. The results are equivalent to those obtained by using the expressions for the energy and angular momentum.

In Sec. III, we showed that the linear velocity of a test particle in a RN spacetime can be written as

$$v_{\epsilon}^{\pm} = v_g \left[\Lambda \pm \sqrt{\Lambda^2 - 1 + (\epsilon/\epsilon_0)^2} \right]^{1/2}, \quad (\text{A1})$$

where

$$\Lambda = 1 - \frac{v_g^2}{2} \left(\frac{\epsilon}{\epsilon_0} \right)^2, \quad v_g = \sqrt{\frac{Mr - Q^2}{\Delta}}, \quad (\text{A2})$$

$$\epsilon_0 = \frac{Mr - Q^2}{Q\sqrt{\Delta}}.$$

Then, the conditions for the existence of timelike velocities are

$$\Lambda^2 - 1 + (\epsilon/\epsilon_0)^2 \geq 0, \quad (\text{A3})$$

$$\Lambda \pm \sqrt{\Lambda^2 - 1 + (\epsilon/\epsilon_0)^2} \geq 0, \quad (\text{A4})$$

$$(v_{\epsilon}^{\pm})^2 < 1. \quad (\text{A5})$$

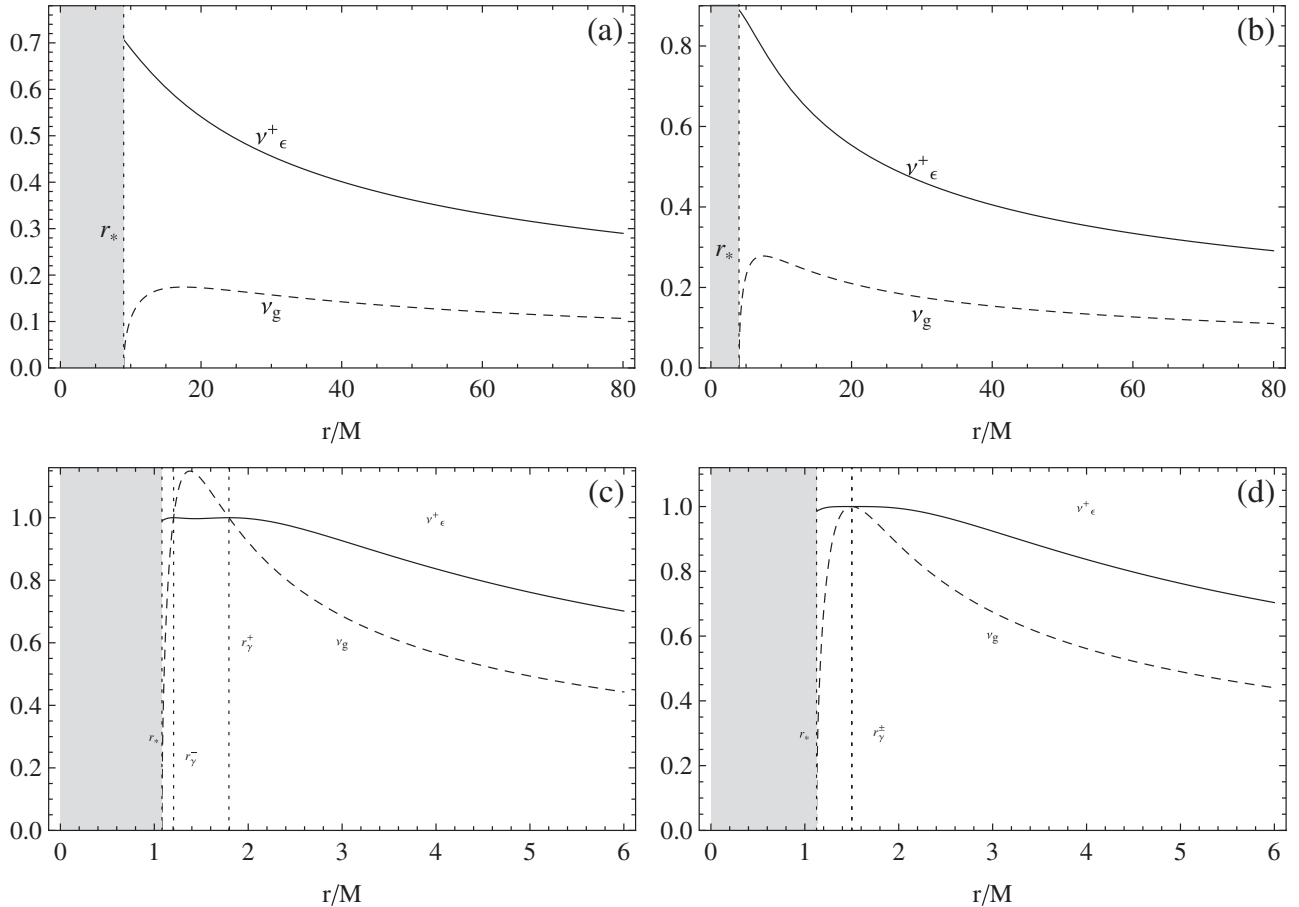


FIG. 33. The positive solution of the linear velocity v_{ϵ}^+ is plotted as a function of the radial distance r/M for different values of the ratios Q/M and ϵ . The geodesic velocity v_g is also shown (dashed curve). Shaded region is forbidden. In (a) the parameter choice is $Q/M = 3$ and $\epsilon = 2$, with $r_* \equiv Q^2/M = 9M$. In (b) the parameter choice is $Q/M = 2$ and $\epsilon = 3$, with $r_* \equiv Q^2/M = 4M$. In (c) the parameter choice is $Q/M = 1.04$ and $\epsilon = 2$, with $r_* \equiv Q^2/M \approx 1.08M$, $r_{\gamma}^+ \equiv [3M + \sqrt{9M^2 - 8Q^2}]/2 \approx 1.79M$, and $r_{\gamma}^- \equiv [3M - \sqrt{9M^2 - 8Q^2}]/2 \approx 1.201M$. In (d) the parameter choice is $Q/M = \sqrt{9/8}$ and $\epsilon = 2$, with $r_* \equiv Q^2/M = (9/8)M$, $r_{\gamma}^{\pm} \equiv [3M \pm \sqrt{9M^2 - 8Q^2}]/2 = (3/2)M$.

We first note that, in the case of a naked singularity, these conditions can be satisfied only for $r \geq Q^2/M$.

For $\epsilon > 1$ and $\epsilon < -1$ the solutions are the geodesic velocities $\nu = \pm \nu_\epsilon^\pm$. In fact, in this case, condition (A4) with the minus sign is no more satisfied. On the other hand, conditions (A3)–(A5) imply that circular timelike orbits exist for $Q/M > \sqrt{9/8}$ in the entire range $r > Q^2/M$. For $1 < Q/M < \sqrt{9/8}$ circular orbits are possible in $r > Q^2/M$ and $r \neq r_\gamma^\pm \equiv [3M \pm \sqrt{9M^2 - 8Q^2}]/2$. Finally, for $Q/M = \sqrt{9/8}$ timelike circular orbits exist for all $r > Q^2/M$, except at $r = (3/2)M$. Moreover, the radii $r = r_\gamma^\pm$ correspond to photon orbits in the RN space-time (see Fig. 33).

Consider now the case $|\epsilon| < 1$. It is useful to introduce here the following notations:

$$r_l^\pm \equiv \frac{3M}{2} \pm \frac{1}{2} \sqrt{9M^2 - 8Q^2 - Q^2\epsilon^2}, \quad (\text{A6})$$

$$\tilde{\epsilon}_\pm \equiv \frac{1}{\sqrt{2}Q} \sqrt{5M^2 \pm 4Q^2 + \sqrt{25M^2 - 24Q^2}}, \quad (\text{A7})$$

and

$$r_s^\pm \equiv \frac{Q^2}{\epsilon^2 Q^2 - M^2} \left[M(\epsilon^2 - 1) \pm \sqrt{\epsilon^2(\epsilon^2 - 1)(M^2 - Q^2)} \right]. \quad (\text{A8})$$

First, consider the case $0 < \epsilon < 1$. For $\epsilon > 0$ condition (33) implies that $r > Q^2/M$. Applying this constraint on conditions (A3) and (A4), we obtain the following results for timelike geodesics.

(1) For $1 < Q/M \leq 5/(2\sqrt{6})$ the following subcases occur:

(a) $0 < \epsilon < \tilde{\epsilon}_-$: Fig. 34(a)

The velocity $\nu = \pm \nu_\epsilon^\pm$ exists in the range $Q^2/M < r \leq r_l^-$ and $r \geq r_l^+$ with $r \neq r_\gamma^\pm$,

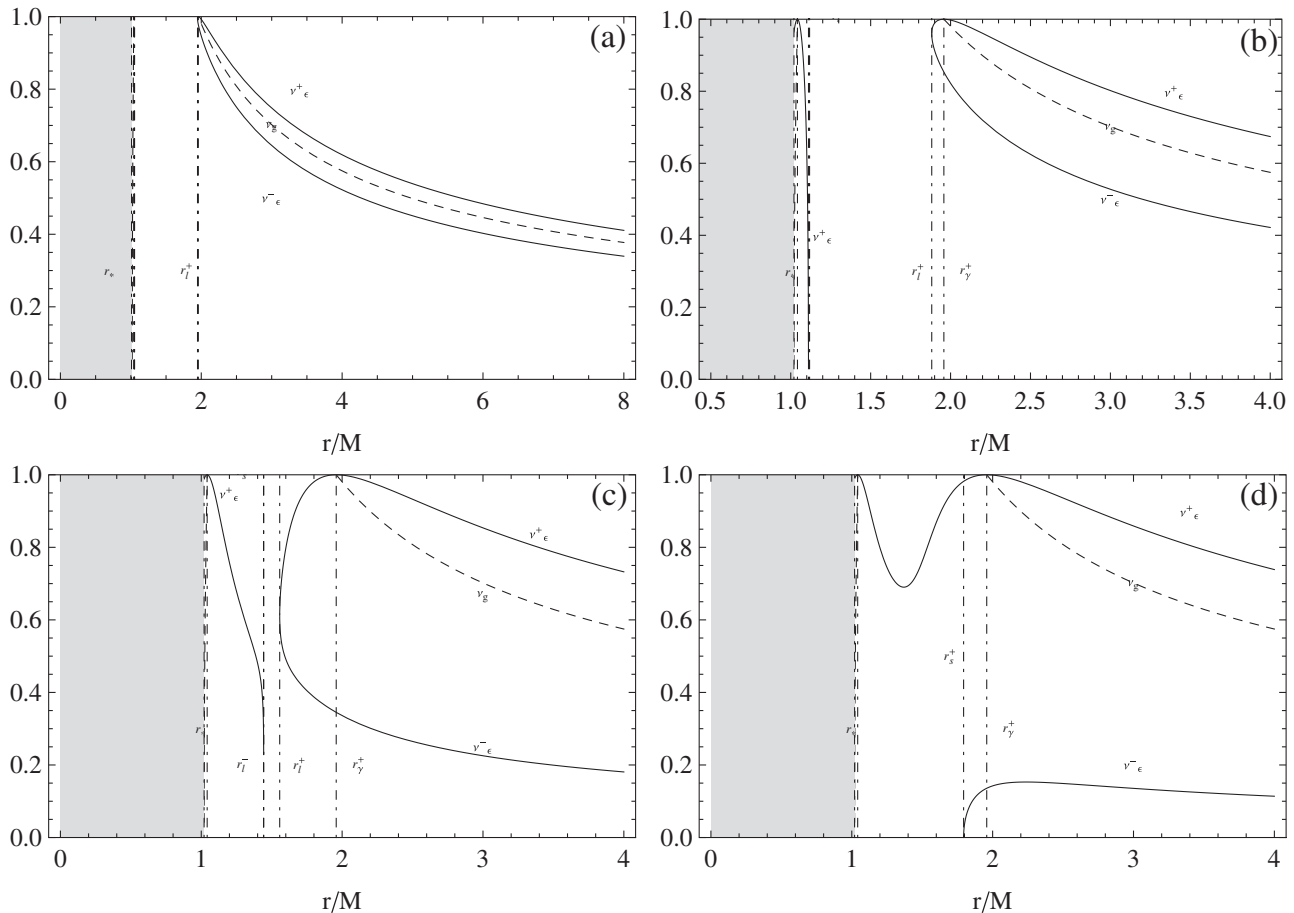


FIG. 34. The positive solution of the linear velocity ν_ϵ is plotted as a function of the radial distance r/M for $Q/M = 1.01$ and different values of the ratio ϵ . In this case $r_\gamma^+ = 1.96M$, $r_\gamma^- = 1.042M$ with $r_* \equiv Q^2/M = 1.02M$, $\tilde{\epsilon}_- = 0.31$, $\tilde{\epsilon}_+ = 0.9$, $\epsilon_l \approx 0.91$. The geodesic velocity ν_g is also shown (dashed curve). Shaded region is forbidden. In (a) the parameter choice is $\epsilon = 0.2$ with $r_s^+ = 1.05M$, and $r_l^+ = 1.95M$, $r_l^- = 1.05M$. In (b) the parameter choice is $\epsilon = 0.5$. Here $r_s^+ = 1.11M$, and $r_l^+ = 1.88M$, $r_l^- = 1.12M$. In (c) the parameter choice is $\epsilon = 0.9$. Here $r_s^+ = 1.11M$, and $r_l^+ = 1.88M$, $r_l^- = 1.12M$. In (d) the parameter choice is $\epsilon = 0.95$. Here $r_s^+ = 1.79M$, and r_l^\pm do not exist.

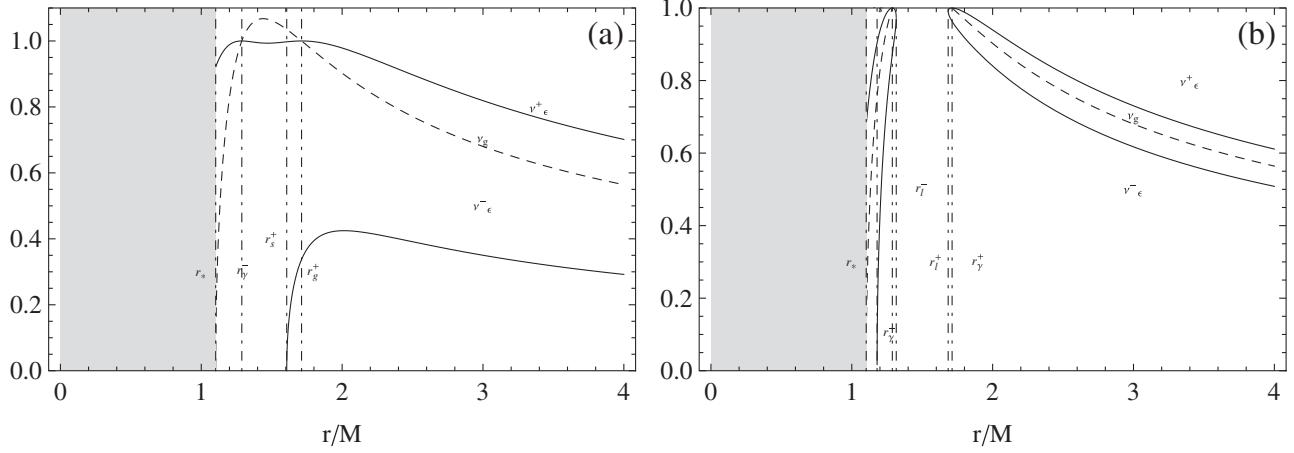


FIG. 35. The positive solution of the linear velocity ν_ϵ is plotted as a function of the radial distance r/M for $Q/M = 1.05$ and different values of the ratio ϵ . In this case $r_\gamma^+ = 1.71M$, $r_\gamma^- = 1.29M$ with $r_* \equiv Q^2/M \approx 1.102M$, $\epsilon_l \approx 0.40$. The geodesic velocity ν_g is also shown (dashed curve). Shaded region is forbidden. In (a) the parameter choice is $\epsilon = 0.7$. Here $r_s^+ = 1.61M$, and r_l^\pm are not defined. In (b) the parameter choice is $\epsilon = 0.2$. Here $r_s^+ = 1.2M$, and $r_l^+ = 1.68M$, $r_l^- = 1.32M$.

- $\nu = \pm \nu_\epsilon^-$ exists in the range $r_s^+ < r \leq r_l^-$ and $r \geq r_l^+$.
- (b) $\tilde{\epsilon}_- \leq \epsilon \leq \tilde{\epsilon}_+$: Fig. 34(b)
 The velocity $\nu = \pm \nu_\epsilon^+$ exists in the range $Q^2/M < r < r_l^-$ and $r \geq r_l^+$ with $r \neq r_\gamma^\pm$, $\nu = \pm \nu_\epsilon^-$ exists in the range $r \geq r_l^+$.
- (c) $\tilde{\epsilon}_+ < \epsilon < \epsilon_l$: Fig. 34(c).
 The velocity $\nu = \pm \nu_\epsilon^+$ exists in the range $Q^2/M < r \leq r_l^-$ and $r \geq r_l^+$ with $r \neq r_\gamma^\pm$, $\nu = \pm \nu_\epsilon^-$ exists in the range $r_s^+ < r \leq r_l^-$ and $r \geq r_l^+$.
- (d) $\epsilon_l \leq \epsilon < 1$: Fig. 34(d)
 The solutions are the geodesic velocities $\nu = \pm \nu_\epsilon^+$ in the range $r > Q^2/M$ with $r \neq r_\gamma^\pm$. The solution $\nu = \pm \nu_\epsilon^-$ exists for $\epsilon_l \leq \epsilon < M/Q$ in the range $r > r_s^+$.
- (2) For $5/(2\sqrt{6}) < Q/M < \sqrt{9/8}$ the following sub-cases occur:
 (a) $0 < \epsilon < \epsilon_l$: Fig. 35(b)
 The velocity $\nu = \pm \nu_\epsilon^+$ exists in the range $Q^2/M < r \leq r_l^-$ and $r > r_l^+$ with $r \neq r_\gamma^\pm$, $\nu = \pm \nu_\epsilon^-$ exists in the range $r_s^+ < r \leq r_l^-$ and $r \geq r_l^+$.
 (b) $\epsilon_l \leq \epsilon < 1$: Fig. 35(a)
 The velocity $\nu = \pm \nu_\epsilon^+$ exists in the range $r > Q^2/M$, $\nu = \pm \nu_\epsilon^-$ exists in the range $r > r_s^+$.
- (3) $Q/M \geq \sqrt{9/8}$: Figs. 36 and 37.
 The velocity $\nu = \pm \nu_\epsilon^+$ exists in the range $r > Q^2/M$ for $Q/M > \sqrt{9/8}$ whereas for $Q/M = \sqrt{9/8}$ this is a solution in $r/M > 9/8$ with $r/M \neq 3/2$, $\nu = \pm \nu_\epsilon^-$ exists for $0 < \epsilon < M/Q$ in the range $r > r_s^+$.

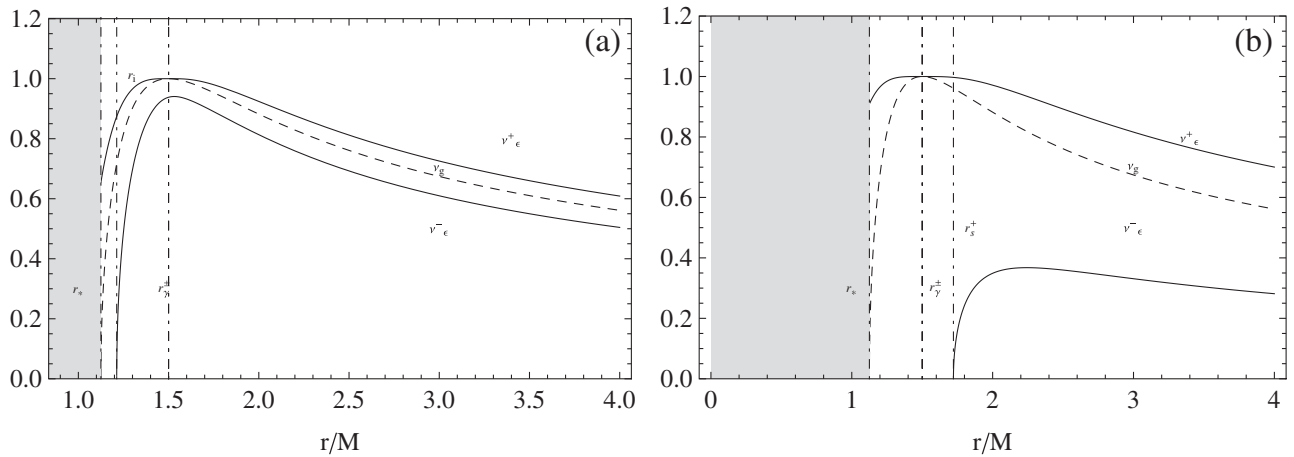


FIG. 36. The positive solution of the linear velocity ν_ϵ is plotted as a function of the radial distance r/M for $Q/M = \sqrt{9/8}$ and different values of the ratio ϵ . In this case $r_\gamma^+ = r_\gamma^- = 3/2M$ with $r_* \equiv 9/8M$, $\epsilon_l = 0$. The geodesic velocity ν_g is also shown (dashed curve). Shaded region is forbidden. In (a) the parameter choice is $\epsilon = 0.2$ with $r_s^+ = 1.2M$. In (b) the parameter choice is $\epsilon = 0.7$ with $r_s^+ = 1.72M$.

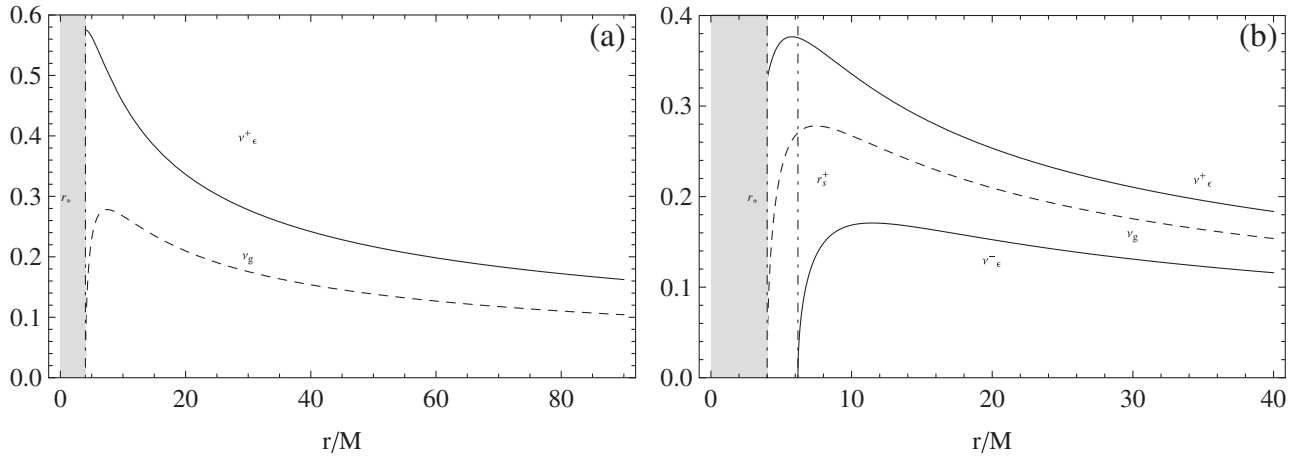


FIG. 37. The positive solution of the linear velocity v_ϵ is plotted as a function of the radial distance r/M for $Q/M = 2$ and different values of the ratio ϵ . In this case $r_* \equiv Q^2/M \approx 4M$. The geodesic velocity v_g is also shown (dashed curve). Shaded region is forbidden. In (a) the parameter choice is $\epsilon = 0.7$ with $r_s^+ = 1.48M$. In (b) the parameter choice is $\epsilon = 0.2$ with $r_s^+ = 6.2M$.

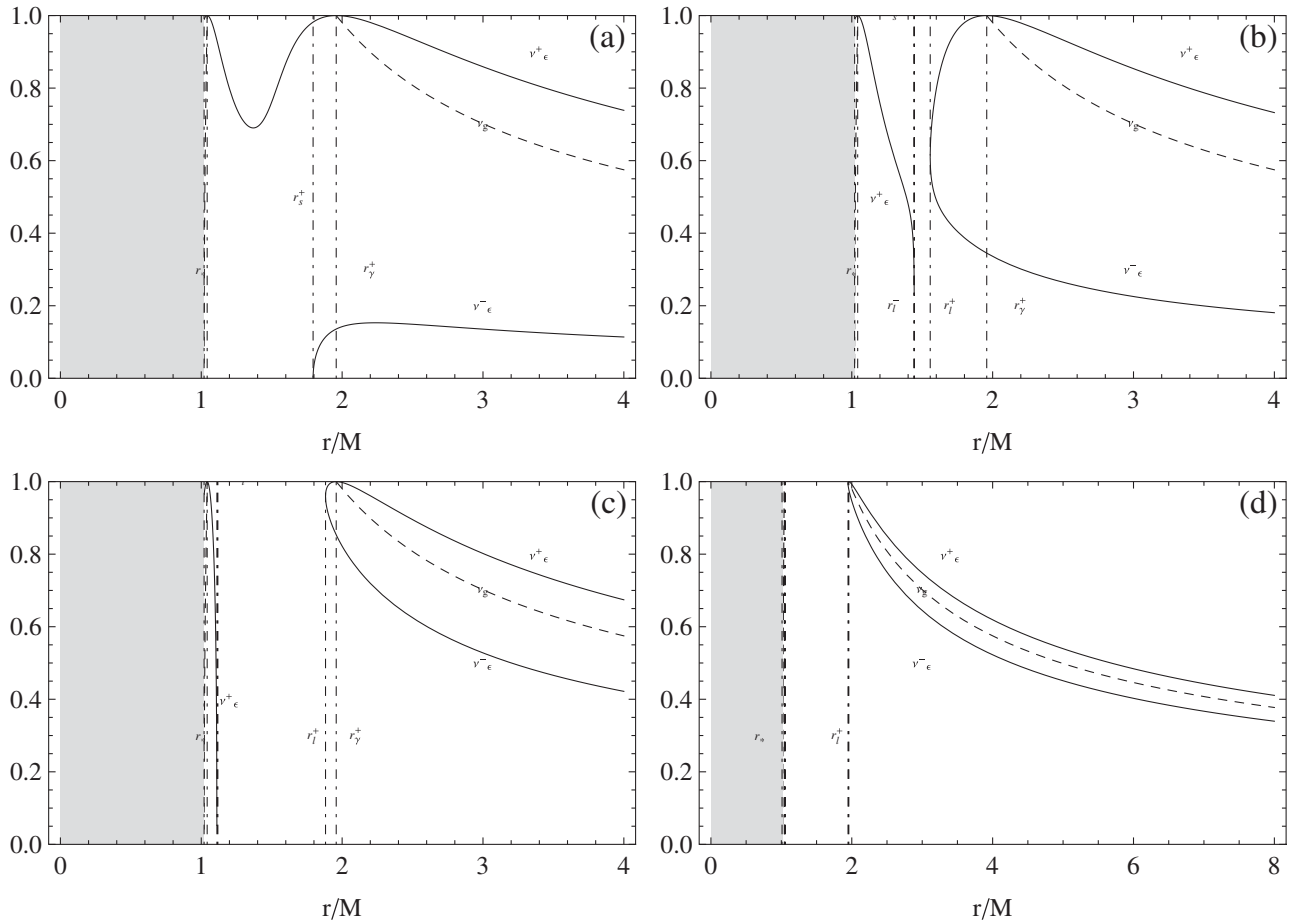


FIG. 38. The positive solution of the linear velocity v_ϵ is plotted as a function of the radial distance r/M for $Q/M = 1.01$ and different values of the ratio ϵ . In this case $r_s^+ = 1.96M$, $r_s^- = 1.042M$, $r_* \equiv Q^2/M = 1.02M$, $\tilde{\epsilon}_- = 0.31$, $\tilde{\epsilon}_+ = 0.9$, and $\epsilon_l \approx 0.91$. The geodesic velocity v_g is also shown (dashed curve). Shaded region is forbidden. In (a) the parameter choice is $\epsilon = -0.95$. Here $r_s^+ = 1.79M$, and r_l^\pm do not exist. In (b) the parameter choice is $\epsilon = -0.9$. Here $r_s^+ = 1.11M$, $r_l^+ = 1.88M$, and $r_l^- = 1.12M$. In (c) the parameter choice is $\epsilon = -0.5$. Here $r_s^+ = 1.11M$, $r_l^+ = 1.88M$, and $r_l^- = 1.12M$. In (d) the parameter choice is $\epsilon = -0.2$. Here $r_s^+ = 1.05M$, $r_l^+ = 1.95M$, and $r_l^- = 1.05M$.

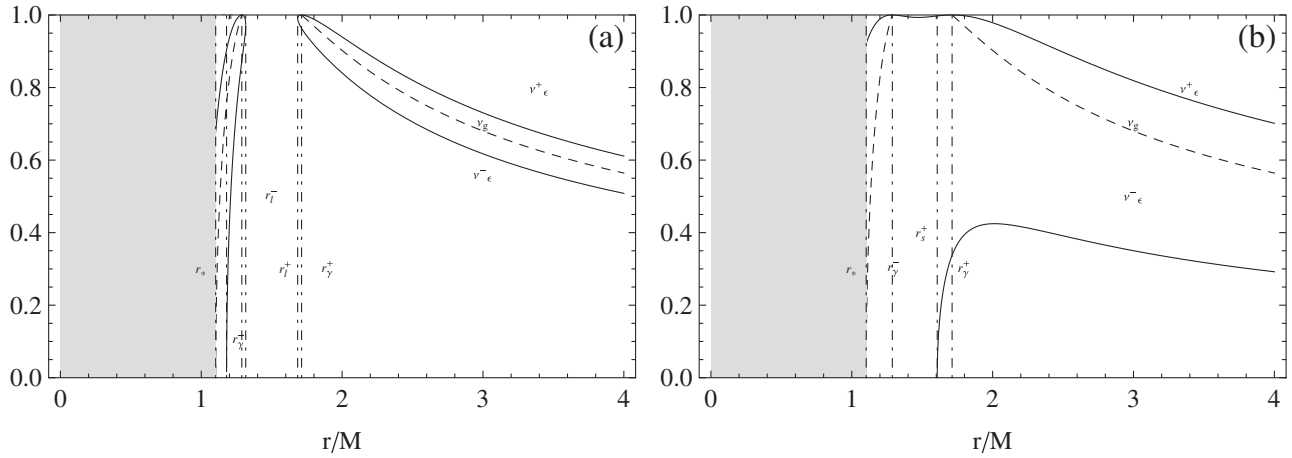


FIG. 39. The positive solution of the linear velocity v_ϵ is plotted as a function of the radial distance r/M for $Q/M = 1.05$ and different values of the ratio ϵ . In this case $r_\gamma^+ = 1.71M$, $r_\gamma^- = 1.29M$, $r_* \equiv Q^2/M \approx 1.102M$, and $\epsilon_l \approx 0.40$. The geodesic velocity v_g is also shown (dashed curve). Shaded region is forbidden. In (a) the parameter choice is $\epsilon = -0.2$. Here $r_s^+ = 1.2M$, $r_l^+ = 1.68M$, and $r_l^- = 1.32M$. In (b) the parameter choice is $\epsilon = -0.7$. Here $r_s^+ = 1.61M$, and r_l^\pm are not defined.

The results for $-1 < \epsilon < 0$ are summarized below.

(1) For $1 < Q/M \leq 5/(2\sqrt{6})$ the following subcases occur:

- (a) For $-1 < \epsilon \leq -\epsilon_l$, the velocity $v = \pm v_\epsilon^+$ exists in the range $r > Q^2/M$ with $r \neq r_\gamma^\pm$, $v = \pm v_\epsilon^-$ exists for $-(M/Q) < \epsilon \leq -\epsilon_l$ in the range $r > r_s^+$ [see Fig. 39(a)].
- (b) For $-\epsilon_l < \epsilon < -\tilde{\epsilon}_+$, the solution is $v = \pm v_\epsilon^+$ in the range $Q^2/M < r \leq r_l^-$ and $r \geq r_l^+$ with $r \neq r_\gamma^\pm$, $v = \pm v_\epsilon^-$ exists in the range $r_s^+ < r \leq r_l^-$ and $r \geq r_l^+$ [see Fig. 39(b)].
- (c) For $-\tilde{\epsilon}_+ \leq \epsilon \leq -\tilde{\epsilon}_-$, the velocity $v = \pm v_\epsilon^-$ exists in the range $r \geq r_l^+$. $v = \pm v_\epsilon^+$ exists for $-\tilde{\epsilon}_+ < \epsilon < -\tilde{\epsilon}_-$ in the range $(Q^2/M) <$

- $r < r_s^+$, and $r \geq r_l^+$ with $r \neq r_\gamma^\pm$, and for $\epsilon = -\tilde{\epsilon}^\pm$ the velocity v_ϵ^+ exists for $Q^2/M < r < r_l^-$ and $r \geq r_l^+$ with $r \neq r_\gamma^\pm$. Finally, for $Q = 5/(2\sqrt{6})M$ and $\epsilon = -\tilde{\epsilon}_+$, v_ϵ^+ exists for $(Q^2/M) < r < r_l^-$, and $r \geq r_l^+$ [see Fig. 38(c)].
- (d) For $-\tilde{\epsilon}_- < \epsilon < 0$, the solutions are the geodesic velocities $v = \pm v_\epsilon^+$ in the range $(Q^2/M) < r \leq r_l^-$ and $r \geq r_l^+$ with $r \neq r_\gamma^\pm$. The solution $v = \pm v_\epsilon^-$ exists in $r_s^+ < r \leq r_l^-$ and $r \geq r_l^+$ [see Fig. 38(d)].

(2) For $5/(2\sqrt{6}) < Q/M < \sqrt{9/8}$ the following subcases occur:

- (a) For $-1 < \epsilon \leq -\epsilon_l$, the velocity $v = \pm v_\epsilon^+$ exists in the range $r > Q^2/M$ with $r \neq r_\gamma^\pm$,

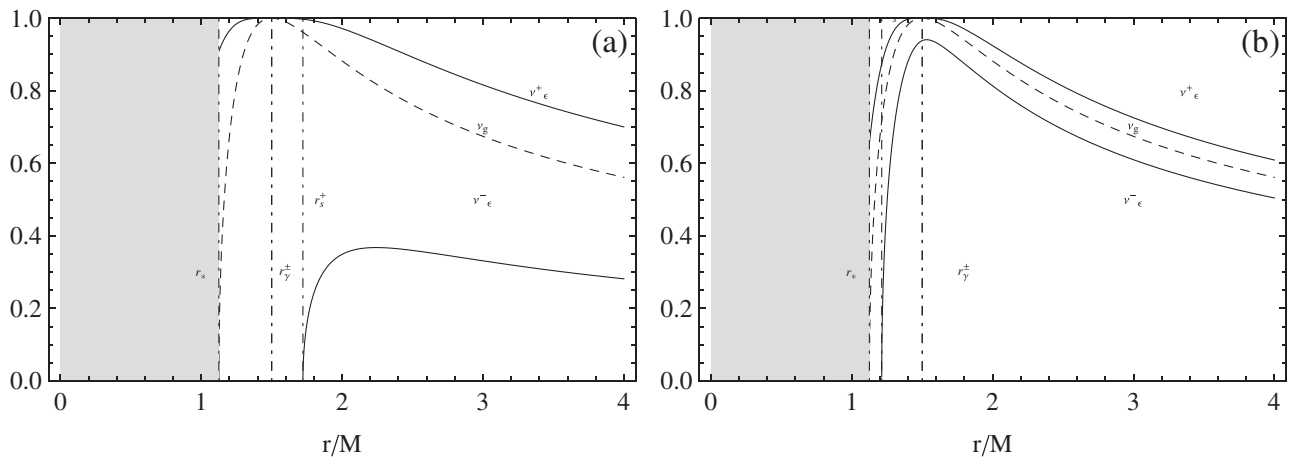


FIG. 40. The positive solution of the linear velocity v_ϵ is plotted as a function of the radial distance r/M for $Q/M = \sqrt{9/8}$ and different values of the ratio ϵ . In this case $r_\gamma^+ = r_\gamma^- = 3/2M$, $r_* \equiv 9/8M$, and $\epsilon_l = 0$. The geodesic velocity v_g is also shown (dashed curve). Shaded region is forbidden. In (a) the parameter choice is $\epsilon = -0.7$ with $r_s^+ = 1.72M$. In (b) the parameter choice is $\epsilon = -0.2$ with $r_s^+ = 1.2M$.

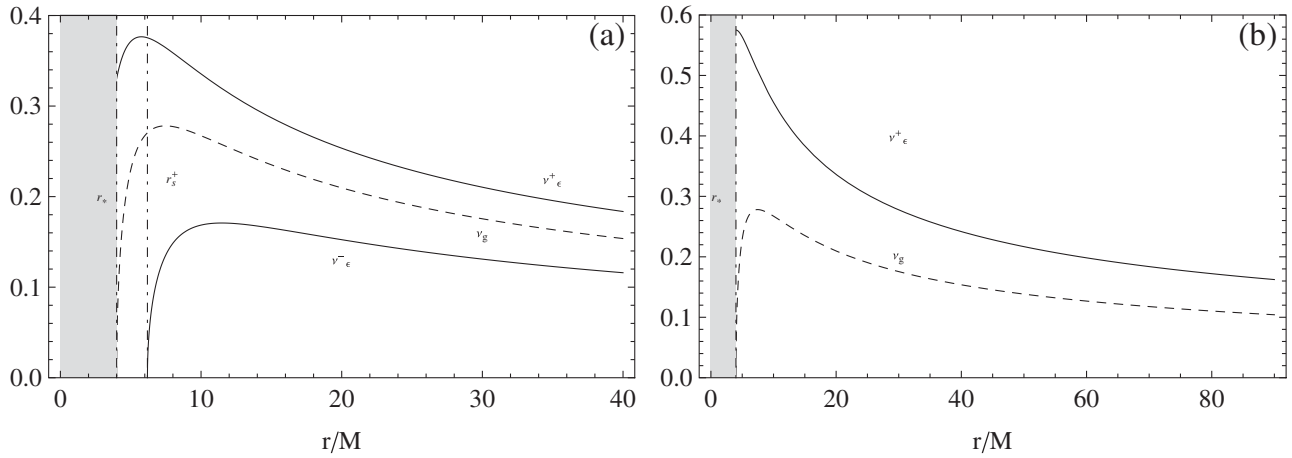


FIG. 41. The positive solution of the linear velocity ν_ϵ is plotted as a function of the radial distance r/M for $Q/M = 2$ and different values of the ratio ϵ . In this case $r_* \equiv Q^2/M \approx 4M$. The geodesic velocity ν_g is also shown (dashed curve). Shaded region is forbidden. In (a) the parameter choice is $\epsilon = -0.2$. Here $r_s^+ = 6.2M$. In (b) the parameter choice is $\epsilon = -0.7$. Here $r_s^+ = 1.48M$.

- $\nu = \pm \nu_\epsilon^-$ exists for $-(M/Q) < \epsilon \leq -\epsilon_l$ in the range $r > r_s^+$ [see Fig. 39(b)].
- (b) For $-\epsilon_l \leq \epsilon < 0$, the velocity $\nu = \pm \nu_\epsilon^+$ exists in the range $Q^2/M < r \leq r_l^-$ and $r \geq r_l^+$, $r \neq r_\gamma^\pm$, $\nu = \pm \nu_\epsilon^-$ exists in the range $r_s^+ < r \leq r_l^-$ and $r \geq r_l^+$ [see Fig. 39(a)].
- (3) For $Q/M \geq \sqrt{9/8}$ the velocity $\nu = \pm \nu_\epsilon^-$ exists for $-(M/Q) < \epsilon < 0$ in the range $r > r_s^+$. $\nu = \pm \nu_\epsilon^+$ is a solution for $Q/M > \sqrt{9/8}$ and $-1 < \epsilon < 0$ in $r > Q^2/M$ whereas for $Q/M = \sqrt{9/8}$ this is a solution in $r/M > 9/8$ with $r/M \neq 3/2$ (see Figs. 40 and 41).

- [1] R. Ruffini, *On the Energetics of Black Holes, Le Astres Occlus* (Gordon and Breach, Les Houches, 1972).
- [2] S. Chandrasekhar, *The Mathematical Theory of Black Holes* (Oxford University Press, New York, 1983).
- [3] J. Levin and G. Perez-Giz, *Phys. Rev. D* **77**, 103005 (2008).
- [4] N. Bilic, Proc. Sci., P2GC (2006) 004 [arXiv:astro-ph/0610657].
- [5] S. Grunau and V. Kagramanova, *Phys. Rev. D* **83**, 044009 (2011).
- [6] E. Hackmann, V. Kagramanova, J. Kunz, and C. Lammerzahl, *Phys. Rev. D* **78**, 124018 (2008).
- [7] V. Kagramanova, J. Kunz, E. Hackmann, and C. Lammerzahl, *Phys. Rev. D* **81**, 124044 (2010).
- [8] E. Hackmann, C. Lammerzahl, V. Kagramanova, and J. Kunz, *Phys. Rev. D* **81**, 044020 (2010).
- [9] E. Hackmann, V. Kagramanova, J. Kunz, and C. Lammerzahl, *Europhys. Lett.* **88**, 30008 (2009).
- [10] E. Belbruno and F. Pretorius, arXiv:1103.0585.
- [11] L. Barack and N. Sago, *Phys. Rev. D* **83**, 084023 (2011).
- [12] D. Pugliese, H. Quevedo, and R. Ruffini, *Phys. Rev. D* **83**, 024021 (2011).
- [13] D. Pugliese, H. Quevedo, and R. Ruffini, in *Proceedings of MG12, Marcel Grossman Meetin, Paris, 2009* (World Scientific, Singapore, 2011).
- [14] K. S. Virbhadra and G. F. R. Ellis, *Phys. Rev. D* **65**, 103004 (2002).
- [15] K. S. Virbhadra and C. R. Keeton, *Phys. Rev. D* **77**, 124014 (2008).
- [16] M. P. Dabrowski and J. Osarczuk, *Astrophys. Space Sci.* **229**, 139 (1995).
- [17] M. P. Dabrowski and I. Prochnicka, *Phys. Rev. D* **66**, 043508 (2002).
- [18] V. Balek, J. Bicak, and Z. Stuchlik, *Bulletin of the Astronomical Institutes of Czechoslovakia* **40**, 133 (1989).
- [19] V. D. Gladush and M. V. Galadgyi, *Kinematics and Physics of Celestial Bodies* **25**, 79 (2009).
- [20] W. B. Bonnor, *Classical Quantum Gravity* **10**, 2077 (1993).
- [21] D. Bini, A. Geralico, and R. Ruffini, *Phys. Rev. D* **75**, 044012 (2007).
- [22] D. Bini, A. Geralico, and R. Ruffini, *Phys. Rev. D* **77**, 064020 (2008).
- [23] D. Bini, A. Geralico, and R. Ruffini, *Phys. Lett. A* **360**, 515 (2007).
- [24] D. Bini, A. Geralico, and F. de Felice, *Int. J. Mod. Phys. D* **14**, 1793 (2005).
- [25] P. Pradhan and P. Majumdar, *Phys. Lett. A* **375**, 474 (2011).
- [26] V. D. Gladush and M. V. Galadgyi, arXiv:1011.0843.
- [27] M. Olivares, J. Saavedra, C. Leiva, and J. R. Villanueva, arXiv:1101.0748.
- [28] O. B. Zaslavskii, *Pisma Zh. Eksp. Teor. Fiz.* **92**, 635 (2010); [*JETP Lett.* **92**, 571 (2010)].

- [29] Ragab M. Gad, *Astrophys. Space Sci.* **330**, 107 (2010).
- [30] G. Dotti and R. J. Gleiser, *Classical Quantum Gravity* **27**, 185007 (2010).
- [31] P. S. Joshi, *Gravitational Collapse and Spacetime Singularities* (Cambridge Monographs on Mathematical Physics, Cambridge, England, 2007).
- [32] V. A. Belinski, M. Pizzi, and A. Paolino, *AIP Conf. Proc.* **1059**, 3 (2008).
- [33] O. Luongo and H. Quevedo, "Toward an Invariant Definition of Repulsive Gravity," in Proceedings of MG12, Marcel Grossman Meeting (to be published).
- [34] M. Pizzi and A. Paolino, *Int. J. Mod. Phys. D* **18**, 1955 (2009).
- [35] V. Belinski, M. Pizzi, and A. Paolino, *Int. J. Mod. Phys. D* **18**, 513 (2009).
- [36] M. Pizzi and A. Paolino, *Int. J. Mod. Phys. A* **23**, 1222 (2008).
- [37] A. Paolino and M. Pizzi, *Int. J. Mod. Phys. D* **17**, 1159 (2008).
- [38] V. S. Manko, *Phys. Rev. D* **76**, 124032 (2007).
- [39] G. A. Alekseev and V. A. Belinski, arXiv:0710.2515.
- [40] G. Preti and F. de Felice, *Am. J. Phys.* **76**, 671 (2008).
- [41] F. de Felice, *Classical Quantum Gravity* **12**, 1119 (1995).
- [42] F. de Felice, *Nuovo Cimento Soc. Ital. Fis. B* **122**, 481 (2007).
- [43] A. N. Aliev, ICTP, 1992 (unpublished).
- [44] J. M. Cohen and R. Gautreau, *Phys. Rev. D* **19**, 2273 (1979).
- [45] E. P. T. Liang, *Phys. Rev. D* **9**, 3257 (1974).
- [46] M. Patil and P. S. Joshi, *Phys. Rev. D* **82**, 104049 (2010).
- [47] M. Patil, P. S. Joshi, and D. Malafarina, *Phys. Rev. D* **83**, 064007 (2011) arXiv:1102.2030.
- [48] A. Qadir and A. A. Siddiqui, *Int. J. Mod. Phys. D* **16**, 25 (2007).
- [49] F. Belgiorno, M. Martellini, and M. Baldicchi, *Phys. Rev. D* **62**, 084014 (2000).
- [50] Z. Kovacs and T. Harko, *Phys. Rev. D* **82**, 124047 (2010).
- [51] F. D. Lora-Clavijo, P. A. Ospina-Henao, and J. F. Pedraza, *Phys. Rev. D* **82**, 084005 (2010).
- [52] D. Vogt and P. S. Letelier, *Phys. Rev. D* **70**, 064003 (2004).
- [53] H. Quevedo, *Gen. Relativ. Gravit.* **43**, 1141 (2010).
- [54] H. Quevedo, arXiv:1012.4030.